Notes for the MIT NUPAX Oral Exam: Detector Physics

Siddharth Narayanan, MIT

Last modified: May 13, 2016

Disclaimer: the author of these notes makes no guarantee that anything in here is remotely correct.

Contents

0 General information **4**
0.1 Momentum measurement of charged particles . . . 4

1 Basic radiation sources **5**

2 Passage of radiation through matter **7**
2.1 Energy loss of heavy charged particles in matter . . . 7
2.2 Cerenkov radiation . . . 9
2.3 Interactions of electrons/positrons in matter . . . 9
2.3.1 Multiple Coulomb scattering . . . 11
2.4 Interaction of photons in matter . . . 11
2.4.1 Photoelectric effect . . . 11
2.4.2 Compton scattering . . . 12
2.4.3 Pair production . . . 13
2.4.4 Photon interaction summary . . . 15
2.4.5 EM showers . . . 15
2.5 Interactions of neutrons in matter . . . 16
2.5.1 Mechanisms of interaction . . . 16
2.5.2 Neutron moderation . . . 17

3 General characteristics of detectors **17**

4 Ionization detectors **17**
4.1 Types of gaseous ionization detectors . . . 17
4.1.1 Resistive plate chamber . . . 18
4.1.2 Ionization chamber . . . 18
4.1.3 Proportional counter . . . 19
4.1.4 Geiger-Müller counter . . . 19
4.2 Ionization and transport in gas . . . 19
4.2.1 Mean number of e^-/ion pairs . . . 19
4.2.2 Recombination and e^--attachment . . . 20
4.2.3 Diffusion . . . 20
4.3 Avalanche multiplication . . . 20
4.4 Pulse formation and shape . . . 21
4.5 Multiwire proportional chamber . . . 22
4.6 Drift chamber . . . 23
4.7 Time projection chamber . . . 24

5 Scintillators **25**
5.1 Organic scintillators . . . 26
5.2 Inorganic crystals . . . 27
5.3 Gas . . . 27
5.4 Pulse shape discrimination for particle ID . . . 27
5.5 Quenching . . . 28
5.6 Electron detection . . . 28
5.7 Photon detection . . . 28
5.8 Neutron detection . . . 28

6 Photomultipliers **29**
6.1 Photocathode . . . 29
6.2 Multiplier dynodes . . . 29
6.3 Gain and voltage supply . . . 29
6.4 Pulse shape . . . 30
6.5 Time resolution and response . . . 30
6.5.1 Geometry of PMT . . . 30
6.5.2 Noise . . . 30

7 Semiconductor detectors **31**
7.1 Basic principles . . . 31
7.2 Doped semiconductors . . . 32
7.3 The np junction and depletion zone . . . 33
7.4 Semiconductors as detectors . . . 34
7.4.1 Reverse bias . . . 35
7.4.2 Detector characteristics . . . 35
7.5 Silicon strip detectors . . . 35
7.6 Silicon photomultipliers . . . 36

8 Compact Muon Solenoid **36**
8.1 Silicon tracker . . . 37
8.1.1 Inner pixel detector . . . 37
8.1.2 Outer strip detector . . . 38
8.1.3 Track reconstruction . . . 38
8.1.4 Vertex reconstruction . . . 39
8.2 Electromagnetic calorimeter . . . 39
8.2.1 Barrel configuration . . . 40
8.2.2 Endcap configuration . . . 40
8.2.3 Electron and photon reconstruction . . . 40
8.2.4 Energy resolution . . . 41
8.3 Hadron calorimeter . . . 41
8.3.1 HCAL Barrel . . . 41
8.3.2 HCAL Endcap . . . 42
8.3.3 HCAL Forward . . . 42
8.3.4 HCAL Outer . . . 42
8.3.5 Jet energy resolution . . . 42
8.4 Magnet and return yokes . . . 43
8.5 Muon detectors . . . 43
8.5.1 Drift tubes . . . 43
8.5.2 Resistive plate chambers . . . 44
8.5.3 Cathode strip chambers . . . 44
8.5.4 Muon reconstruction . . . 44
8.6 Triggering and DAQ . . . 45

Appendices **46**

A Bibliography **46**

0 General information

A barn is 10^{-24} cm^2. Consider an incident flux F on a point target (assuming the width of the beam is larger than the target). The differential cross-section is:

$$\frac{d\sigma}{d\Omega}(E,\Omega) = \frac{1}{F}\frac{dN_{\text{scatt.}}}{d\Omega}\left[\frac{1}{\text{N/area}} \times \frac{\text{N}}{\text{solid angle}}\right] \tag{1}$$

Given a flux F incident on a target of area A, numberdensity n, and thickness δx, the number scattered is:

$$N_{\text{scatt.}} = n \cdot A \cdot F \cdot \delta x \cdot \frac{d\sigma}{d\Omega} \tag{2}$$

The probability-per-unit length for an interaction in matter is:

$$\mu = \sigma \cdot N_A \rho / A \tag{3}$$

where A is the atomic mass The natural lifetime is $\tau = \tau_{1/2}/\ln 2$.
Timing resolution of various detector types:

Table 33.1: Typical resolutions and deadtimes of common charged particle detectors. Revised November 2011.

Detector Type	Intrinsinc Spatial Resolution (rms)	Time Resolution	Dead Time
Resistive plate chamber	$\lesssim$10 mm	1 ns (50 ps[a])	—
Streamer chamber	300 μm[b]	2 μs	100 ms
Liquid argon drift [7]	∼175–450 μm	$\sim$ 200 ns	$\sim$ 2 μs
Scintillation tracker	∼100 μm	100 ps/n[c]	10 ns
Bubble chamber	10–150 μm	1 ms	50 ms[d]
Proportional chamber	50–100 μm[e]	2 ns	20-200 ns
Drift chamber	50–100 μm	2 ns[f]	20-100 ns
Micro-pattern gas detectors	30–40 μm	$<$ 10 ns	10-100 ns
Silicon strip	pitch/(3 to 7)[g]	few ns[h]	$\lesssim$50 ns[h]
Silicon pixel	$\lesssim$10 μm	few ns[h]	$\lesssim$50 ns[h]
Emulsion	1 μm	—	—

0.1 Momentum measurement of charged particles

- Typically done by bending the particle in a $\vec{B}$-field perpendicular to the direction of motion
- CMS, for example, has a solenoid that causes helical paths
- In general, the path of a particle looks like:

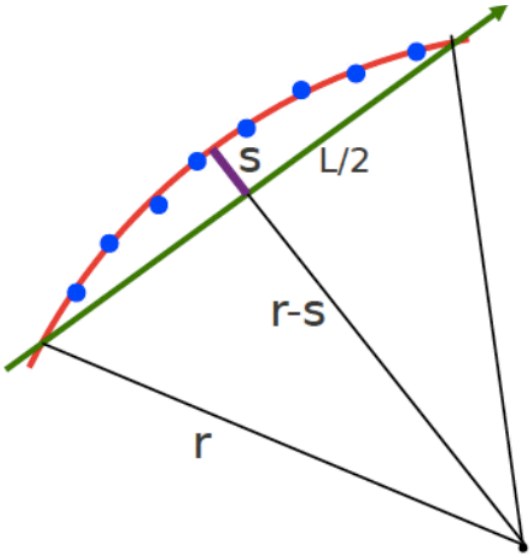

- We can estimate $R \approx L^2/2s$.
- The momentum is then p_T [GeV] $= 0.3 \times B$ [T] $\times R$ [m]
- There are two sources of uncertainty: measurement and multiple scattering
  - Measurement is:
$$\frac{\sigma_{\text{meas.}}}{p_T} = \frac{8\sigma_s}{0.3BL^2}p_T, \quad \sigma_s \propto \frac{\sigma_{r\phi}}{\sqrt{N+4}} \tag{4}$$
    Note the uncertainty is larger for high-momentum particles (the track is straighter)
  - Multiple scattering is:
$$\frac{\sigma_{\text{MS}}}{p_T} = \frac{0.045}{B}\sqrt{\frac{L}{X_0}} \tag{5}$$
  - The use of denser materials and a shorter tracker increases the MS component of the uncertainty

1 Basic radiation sources

- α-decay: $(Z, A) \to (Z-2, A-4) + \alpha$
  - Can be thought of as tunneling through nuclear potential
  - $\Rightarrow$ narrow energy range ($\sim 4-6$ MeV)
  - Higher energy $\Rightarrow$ higher tunneling probability. Therefore, most α-decays are to the ground state (highest ΔE)
  - Large charge: α particles only pass through few cm of air
- β-decay: $n \to p + e^- + \bar{\nu}$, $p \to n + e^+ + \nu$
  - Because 3-body decay, there is a continuous spectrum for e energy
  - Typically goes to an excited nuclear state which decays by γ-radiation
  - Electron capture: $p + e^- \to n + \nu$
    - Observed by looking for γ from e^- filling hole left by captured e^-
  - For tritium, the beta particle energy is < 20 keV

- γ-emission: nucleus de-excites, emitting a γ
  - Selection rules: needs to be $\Delta S = 1$
  - $\mathcal{O}(0.1 - 1)$ MeV
  - Typically happens quickly, but sometimes the transition is spin-suppressed (i.e. if need two γs to get desired $\Delta S = 2$ and $\Delta S = 1$ state is higher energy)
  - Spin-suppressed $\Rightarrow$ lifetimes up to $\mathcal{O}(1)$ years
- Annihilation: $e^- + e^+ \to 2\gamma$, (511 keV each)
  - e^+ from a β^+ process, which interacts with e^- in absorber or detector
  - Signature is sharp peak at $E_\gamma = 511$ keV. Photons are emitted back-to-back typically
- Internal conversion: like γ-emission, but energy from nuclear de-excitation goes to an atomic e^- instead
  - e^- is ejected from shell
  - Typically K-shell electron
  - Useful source of monoenergetic electrons for calibration
- Neutron sources: $(Z, A) \to (Z_1, A_1) + (Z_2, A_2) + n + n + \cdots$
  - Fission products will undergo β, γ decay themselves
  - $$\frac{dN}{dE} = \sqrt{E} \exp\left[-\frac{E}{T}\right] \tag{6}$$
    where E = energy of neutron, T = characteristic energy for that decay $\sim$ MeV
  - Above is for *spontaneous* fission (i.e. no extra energy added to nucleus to cause fission)
- Nuclear reactions: $A + \alpha \to B + n$ or $A + \gamma \to B + n$
  - e.g. $\alpha + {}^9\text{Be} \to {}^{13}\text{C}^*$, where C^* decays by n, α or $3\alpha + n$
  - Typically get $\mathcal{O}(100)$ neutrons per 10^6 αs, depending on the source
  - Neutron energy gets smeared quite a bit in decay

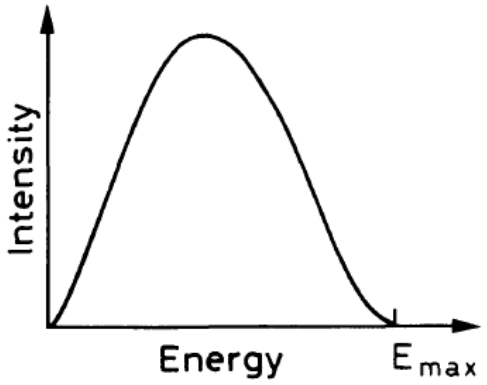

Fig. 1.2. Typical continuous energy spectrum of beta decay electrons

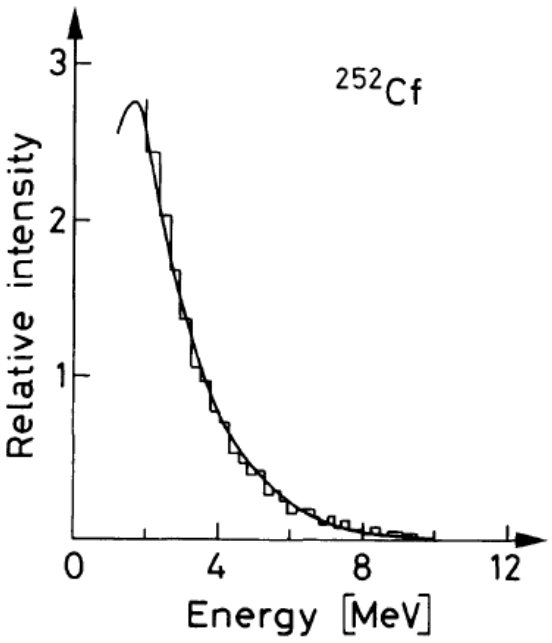

Fig. 1.5. Neutron energy spectrum from ^{252}Cf (from *Lorch* et al. [1.2]). The form of the spectrum can be described by a Maxwellian distribution

2 Passage of radiation through matter

- The probability of at least one interaction over a distance x is $P(x) = 1 - \exp[-n\sigma x]$, where n is the number density of targets
  - $\Rightarrow$ mean free path $\lambda = 1/n\sigma$

2.1 Energy loss of heavy charged particles in matter

- Anything heavier than m_e
- Interactions are with atomic e^- primarily: $\sigma \sim 10^7$-10^8 b
- Either excite (soft) or eject (hard) the e^-
  - e^- from hard interactions can cause secondary ionization
- Quantity of interest is $-\langle dE/dx \rangle$, assuming large fluctuations are very unlikely (untrue for e)
- Bohr's classical calculation:
  - Assuming the impact parameter between the charged particle (charge z) moving at velocity v and the e^- is b:

$$I = \frac{2ze^2}{bv} \Rightarrow \Delta E(b) = \frac{I^2}{2m_e} = \frac{2z^2e^4}{m_e v^2 b^2}$$
$$\Rightarrow -\frac{dE}{dx} = \frac{4\pi z^2 e^4}{m_e v^2} N_e \ln \frac{\gamma^2 m v^3}{ze^2\bar{\nu}} \tag{7}$$

- where $\bar{\nu}$ is the average frequency of bound state electrons.
- The value of dE/dx is gotten by integrating over a reasonable range for b
- Valid for very heavy particles (like α), but not for protons, etc, because quantum effects

- Bethe-Bloch:
  -
$$-\left\langle \frac{dE}{dx} \right\rangle \propto \rho \frac{Z}{A} \frac{z^2}{\beta^2} \left[\ln \left(\frac{2m_e \gamma^2 \beta^2 W_{\max}}{I^2} \right) - 2\beta^2 - \delta - 2\frac{C}{Z} \right] \tag{8}$$

    where:
    * $W_{\max}$ is the maximum energy transfer kinematically allowed
    * I is the mean excitation potential (material-dependent)
    * δ is the density correction (at high β). Corrects for the charged particle polarizing the medium as it travels through (stronger effect for high density). This cancels the quadratic rise from the β^2 term
    * C/Z is the shell-effect. Corrects for case when the incident particle is slow relative to the electron orbital velocity
  - Important features:
    * Minimum ionizing particle occurs at $\beta \sim 0.96 \Rightarrow \gamma \sim 3.6$ (independent of the particle)
    * dE/dx goes down as a function of β at low energies: slow particles feel atomic electric field for longer
    * But then the β^2 relativistic effect causes a rise at high energies: Lorentz contraction of $\vec{E}$-field makes transverse component (wrt particle motion) larger.
    * The quadratic rise in β is canceled by the δ ionization term. Cancellation is stronger for denser materials.

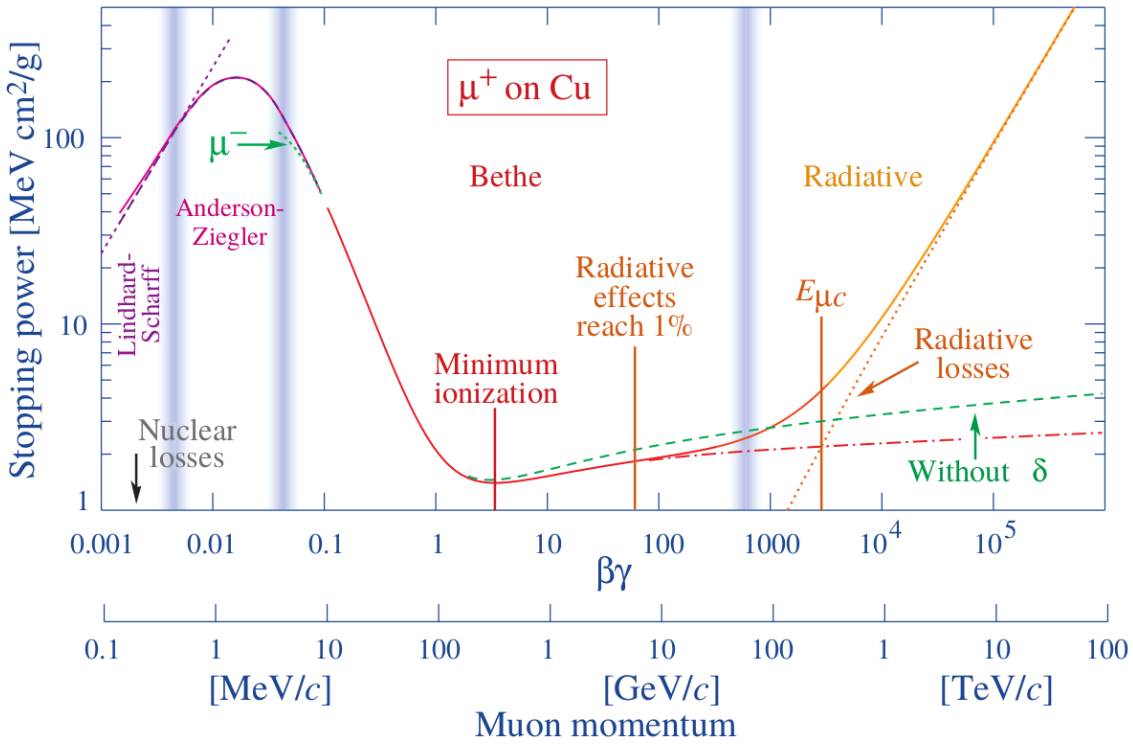

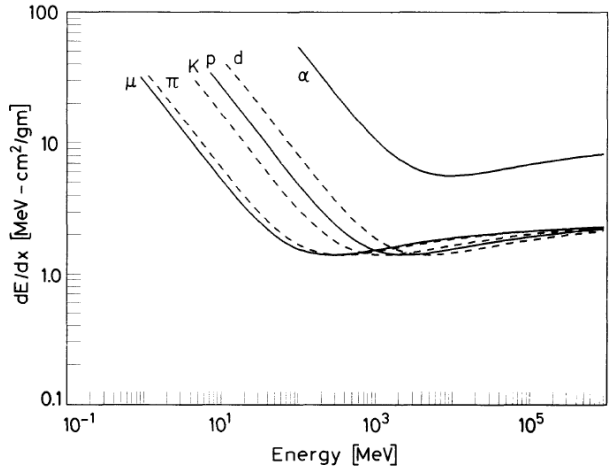

Fig. 2.4. The stopping power *dE/dx* as function of energy for different particles

– Note that the particle is more ionizing at low E $\Rightarrow$ more ionization occurs at end of path

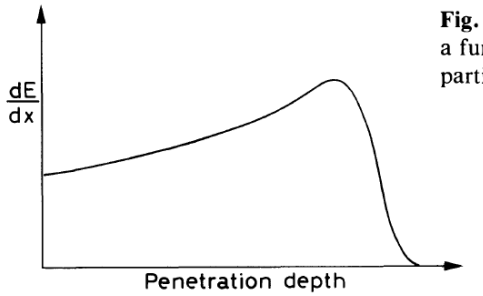

Fig. 2.5. A typical Bragg curve showing the variation of *dE/dx* as a function of the penetration depth of the particle in matter. The particle is more ionizing towards the end of its path

– For a fixed medium:
  * $\frac{dE}{dx} = z^2 f(\beta)$
  * $\Rightarrow$ if $\frac{dE}{dx}$ is known for one particle, it is known for all particles (just have to scale z^2 and calculate new β as a function of energy, mass)

2.2 Cerenkov radiation

- Speed of light in medium is c/n
- If $\beta > 1/n$, a cone of light is observed at an angle θ_C
- $\cos\theta_C = (\beta n(\nu))^{-1}$ (ν is the frequency of the radiation)
- The energy loss is:

$$-\frac{dE}{dx} = z^2 \frac{\alpha\hbar}{c} \int d\nu \left[\nu \left(1 - (\beta n(\nu))^{-2}\right)\right]$$

$$\Longleftrightarrow$$

$$\frac{d^2 N_\gamma}{d\nu dx} = \frac{z^2\alpha}{c}\left(1 - (\beta n(\nu))^{-2}\right) \tag{9}$$

2.3 Interactions of electrons/positrons in matter

- Bremsstrahlung becomes dominant at $E > E_c \sim \mathcal{O}(10)$ MeV. Below this, collisions are dominant (described by Bethe-Bloch)

- Bremsstrahlung cross-section is $\propto (e^2/m)^2 \quad \Rightarrow$ for particles with high m, bremsstrahlung doesn't become relevant until very very high E
  - Kicks in at lower E for $e^{\pm}$

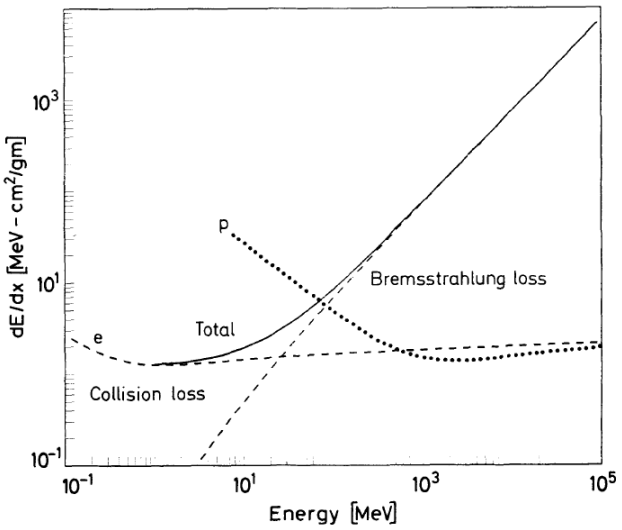

Fig. 2.10. Radiation loss vs. collision loss for electrons in copper. For comparison, the *dE/dx* for protons is also shown

- E_c is defined as the energy at which dE/dx due to collision and brem are the same. An empirical formula is:

$$E_c = \frac{800 \text{ MeV}}{Z + 1.2} \tag{10}$$

- For muons, E_c is $\sim$ TeV (for low Z) to $\sim$ 100 GeV (high Z)
- Radiation length: distance over a particle's energy is reduced by $1/e$. Call it L_{rad}
  - $E = E_0 \exp[-x/L_{\text{rad}}]$

Table 2.2. Critical energies of some materials

Material	Critical energy [MeV]
Pb	9.51
Al	51.0
Fe	27.4
Cu	24.8
Air (STP)	102
Lucite	100
Polystyrene	109
NaI	17.4
Anthracene	105
H_2O	92

Table 2.3. Radiation lengths for various absorbers

Material	[gm/cm^2]	[cm]
Air	36.20	30050
H_2O	36.08	36.1
NaI	9.49	2.59
Polystyrene	43.80	42.9
Pb	6.37	0.56
Cu	12.86	1.43
Al	24.01	8.9
Fe	13.84	1.76
BGO	7.98	1.12
BaF_2	9.91	2.05
Scint.	43.8	42.4

Typical values for X_0, E_c and R_M of materials used in calorimeter

	X_0 [cm]	E_c [MeV]	R_M [cm]
Pb	0.56	7.2	1.6
Scintillator (Sz)	34.7	80	9.1
Fe	1.76	21	1.8
Ar (liquid)	14	31	9.5
BGO	1.12	10.1	2.3
Sz/Pb	3.1	12.6	5.2
PB glass (SF5)	2.4	11.8	4.3

- Because of low mass, variance in dE/dx is larger for $e^{\pm}$ than for heavier particles (long tail from large energy transfers)

2.3.1 Multiple Coulomb scattering

- Elastic scattering off nuclei
- Very little energy loss since $m_A \gg m$ typically
- Rutherford formula:

$$\frac{d\sigma}{d\Omega} = z^2 Z^2 \left(\frac{\alpha\hbar c}{T}\right)^2 \frac{1}{\sin^4(\theta/2)} \tag{11}$$

  - T is the kinetic energy
  - Largest probability for small deflections

- Multiple ($N_{\text{scatt.}} > 20$) scatterings can be treated statistically
  - Assume $P(\theta)$ is Gaussian centered at 0 (this ignores large deflections in the tails)
  - $\langle\theta^2\rangle \sim 10^{-3}$ rad^2 for typical materials
  - Not valid for $e^{\pm}$ which have low mass $\Rightarrow$ large deflections (like backscattering) possible

2.4 Interaction of photons in matter

2.4.1 Photoelectric effect

- γ+atom $\rightarrow$ ion+e^-
- $E_e = h\nu - \phi$, ϕ is the binding energy
- σ decreases as $h\nu$ increases, with a jump up when $h\nu$ reaches a shell binding energy
- $\sigma \sim \mathcal{O}(10^{-1} - 10^4)$ b and is proportional to Z^α, for $\alpha = 4 - 5$ (exact value is a function of $h\nu$)

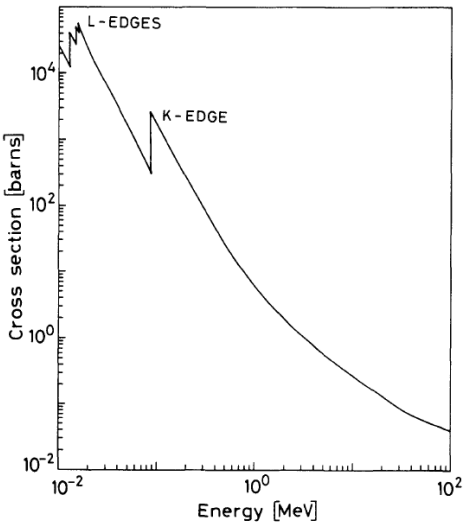

Fig. 2.21. Calculated photoelectric cross section for lead

2.4.2 Compton scattering

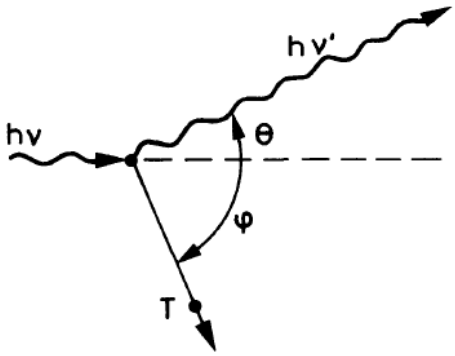

Fig. 2.22. Kinematics of Compton scattering

- Kinematics

$$\lambda' - \lambda = \frac{1}{\nu'} - \frac{1}{\nu} = \frac{h}{m_e}(1 - \cos\theta)$$
$$\cot\phi = \left(1 + \frac{h\nu}{m_e}\right)\tan\frac{\theta}{2}$$

- Klein-Nishina:

$$\frac{d\sigma}{d\Omega} = \frac{\alpha^2}{2m_e^2}\left(\frac{\nu'}{\nu}\right)^2\left[\frac{\nu'}{\nu} + \frac{\nu}{\nu'} - \sin^2\theta\right] \tag{12}$$
$$\sigma \sim 10^{-4} - 10^{0}\ \text{b}$$

- Can define σ_S (σ_A) as the cross-section of scattered (absorbed) energy:

$$\frac{d\sigma_S}{d\Omega} = \frac{h\nu'}{h\nu}\frac{d\sigma}{d\Omega}, \quad \sigma_A = \sigma - \sigma_S \tag{13}$$

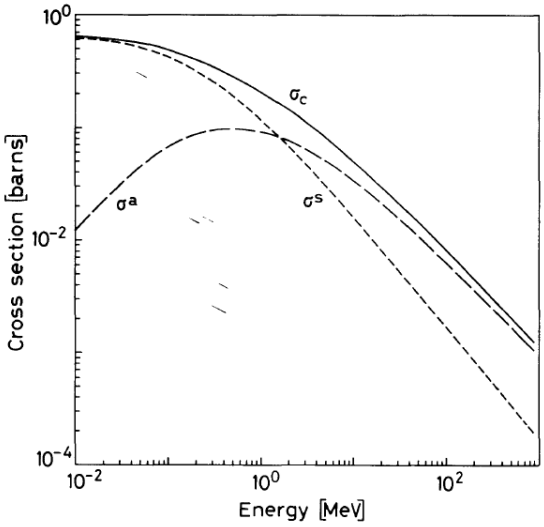

Fig. 2.23. Total Compton scattering cross sections

- Can also define $d\sigma/dT$, where T is the kinetic energy of e^-:

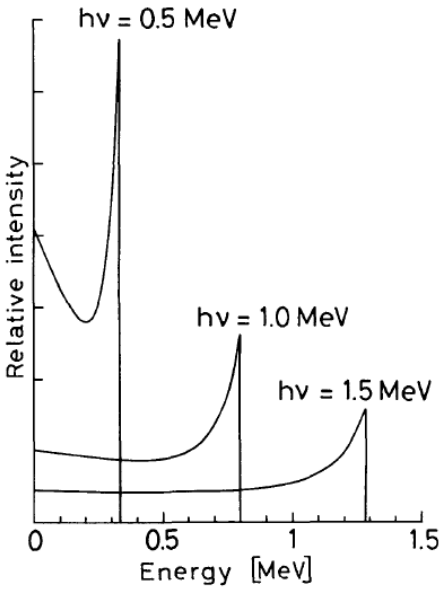

Fig. 2.24. Energy distribution of Compton recoil electrons. The sharp drop at the maximum recoil energy is known as the *Compton edge*

$0 < T < T_{\max}$, where $T_{\max}$ is the max allowed recoil energy:

$$T_{\max} = h\nu \frac{2\xi}{1+2\xi},\ \xi = \frac{h\nu}{m_e} \tag{14}$$

2.4.3 Pair production

- $\gamma \to e^- e^+$
- Mean free path: $\lambda_{\text{pair}} = \frac{9}{7} L_{\text{rad}}$, where $L_{\text{rad}} \sim \mathcal{O}(10)$ cm is for electrons

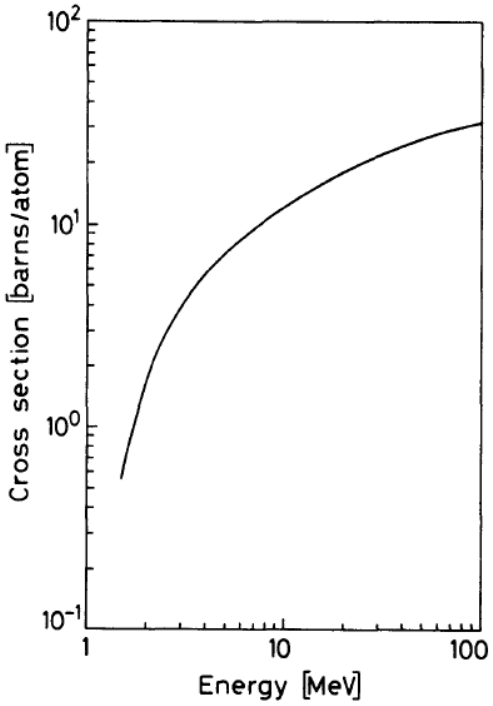

Fig. 2.25. Pair production cross section in lead

2.4.4 Photon interaction summary

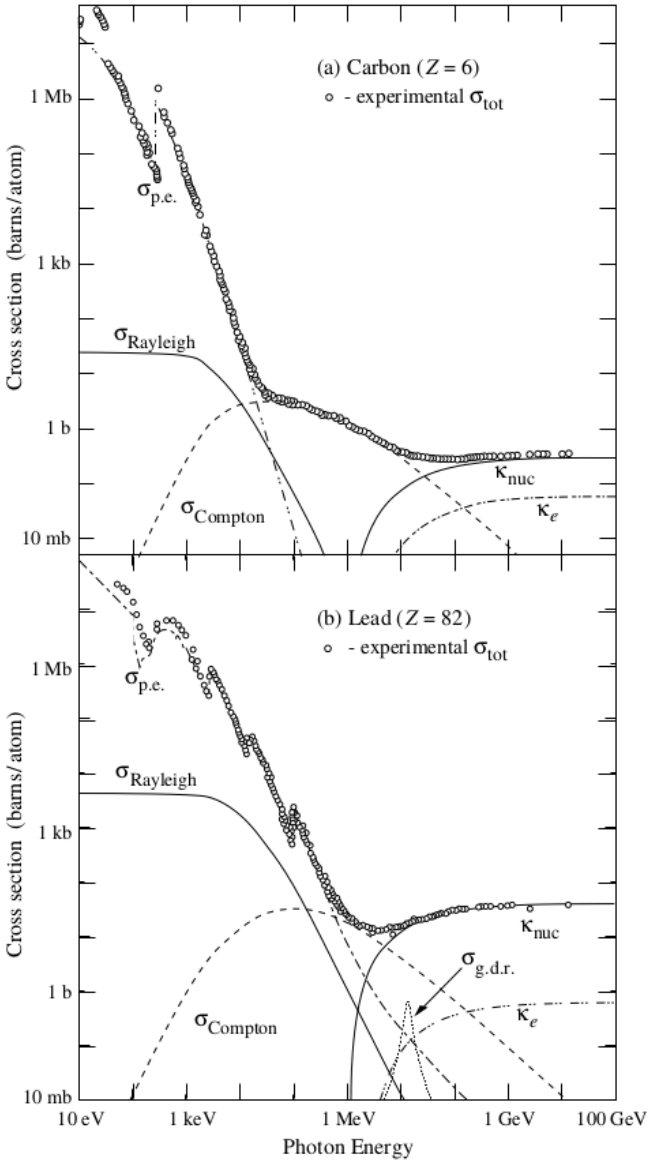

Figure 32.15: Photon total cross sections as a function of energy in carbon and lead, showing the contributions of different processes [51]:

$\sigma_{\text{p.e.}}$ = Atomic photoelectric effect (electron ejection, photon absorption)
σ_{Rayleigh} = Rayleigh (coherent) scattering–atom neither ionized nor excited
σ_{Compton} = Incoherent scattering (Compton scattering off an electron)
κ_{nuc} = Pair production, nuclear field
κ_e = Pair production, electron field
$\sigma_{\text{g.d.r.}}$ = Photonuclear interactions, most notably the Giant Dipole Resonance [52]. In these interactions, the target nucleus is broken up.

Original figures through the courtesy of John H. Hubbell (NIST).

2.4.5 EM showers

- $\gamma \to e^- e^+$, $e^\pm \to e^\pm + \gamma$, $\gamma \to e^- e^+ \cdots$

- Assuming the radiation lengths are $L_\gamma \sim L_e$:
  - $N_{\text{particles}} \sim 2^{x/L}$
  - $E(x) \sim E_0/2^{x/L}$, where E is the energy per particle in the shower at distance x
  - Obviously has to truncate when $E(x) \leq m_e$, but actually stops at $E < E_c$ (no more brem)
  - Let $t = x/L$. Then, $t_{\max} = \ln(E_0/E_c)/\ln 2$ and $N_{\max} \approx E_0/E_c$
    - Need to add correction for particle that induces shower: $t_{\max} = \log_2(E_0/E_c) - C$
    - $C = 0.5$ if γ, else $C = 1$
- Define the Molière radius as the radius of the cylinder surrounding the primary particle that contains 90% of the energy deposited by an EM shower. It satisfies:

$$R_M = X_0 \frac{21.2 \text{ MeV}}{E_c} \tag{15}$$

2.5 Interactions of neutrons in matter

- High energy neutrons: $E > 100$ MeV
- Fast: $\mathcal{O}(100)$ $kev < E < \mathcal{O}(10)$ MeV
- Epithermal: $\mathcal{O}(0.1)$ eV $< E < \mathcal{O}(100)$ keV (where nuclear resonances occur)
- Thermal: $E \sim 1/kT \approx 1/40$ eV
- Ultracold: $E < 0.001$ eV

2.5.1 Mechanisms of interaction

- $A + n \to A + n$: dominant for MeV neutrons (elastic)
- $A + n \to A^* + n'$, $A + n \to B + 2n', \ldots$
  - Neutron must be > 1 MeV to excite the nucleus
  - Inelastic
- Radiative n capture: $n + (Z, A) \to \gamma + (Z, A + 1)$
  - $\sigma \sim 1/v$, so dominant at low energies
  - There can be resonance peaks
- $A + n \to B + p/d/\alpha/t/\alpha p/\cdots$
  - Typically eV $-$ keV
  - $\sigma \sim 1/v$
- Fission (more likely at low [thermal] energies)
- High energy hadron shower
  - Similar to EM shower
  - $E > 100$ MeV

2.5.2 Neutron moderation

- Neutrons bounce around matter, slowing down until at thermal eq. w/ matter
  - Unlikely to be captured by nucleus (or cause fission) at high energies because $\sigma \sim 1/v$ for these processes
- Energy of scattered neutron:

$$\left(\frac{A-1}{A+1}\right)^2 E_0 < E' < E_0 \tag{16}$$

  which implies low A is better for absorbing energy

3 General characteristics of detectors

- Sensitivity to signal is a function of many things:
  - σ of ionizing reactions in the detector
  - Detector mass
  - Material surrounding sensitive volume of detector
- Two continuous responses are considered resolved if separated by a distance greater than the FWHM
- Error is Poissonian for detectors that collect *some* of the particle's energy
  - Error is smaller for detectors that *stop* the particle, since each interaction is not independent
- Define $J = E/W$, so the energy variance is $\sigma^2 = FJ$
  - W =energy lost per ionization in detector
  - F =Fano factor
    - $F = 1 \Rightarrow$ purely Poissonian (e.g. scintillators in which only part of the energy is deposited)
    - $F < 1 \Rightarrow$ better (semiconductors, gases, scintillators which stop the particle)
  - Resolution can be defined two ways:
    - FWHM $= 2.35\frac{\sigma}{J} = 2.35\sqrt{\frac{FW}{E}}$
    - Deviation divided by mean: $\frac{\sigma}{\mu} = \frac{\sigma}{J} = \sqrt{\frac{FW}{E}}$

4 Ionization detectors

4.1 Types of gaseous ionization detectors

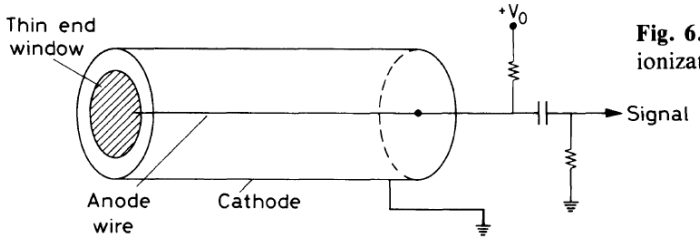

Fig. 6.1. Basic construction of a simple gas ionization detector

- Filled with a noble gas

- Radial $\vec{E}$-field from anode wire to cathode ($\propto 1/\ln(b/a)$, where a is the wire radius and b is the chamber radius)
- Radiation creates e^-/ion pairs in tube
  - If the radiation is charged, this occurs through ionization
  - If neutral, it occurs through secondary ionization (i.e., γ, n ejects an e^- from an atom, which then ionizes the gas)
  - Number of pairs is $\propto E$
  - e^- →anode, ions→cathode
  - Observed signal is a function of V_0:

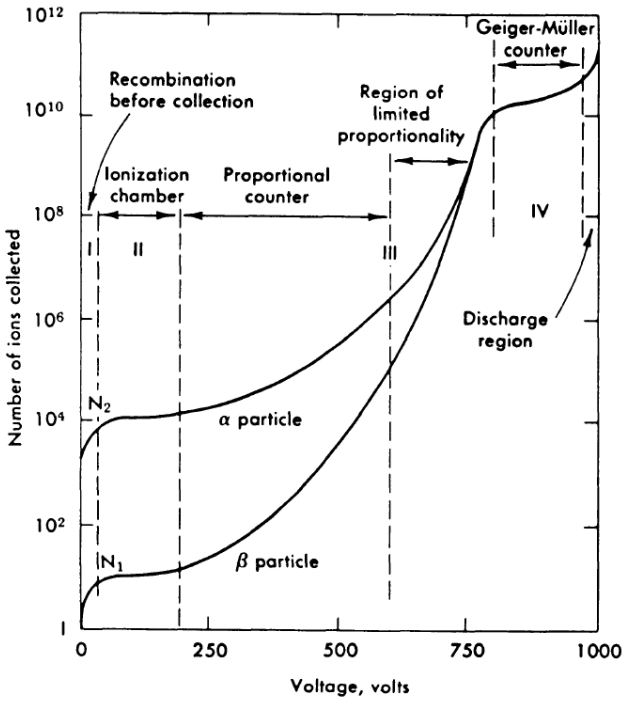

Fig. 6.2. Number of ions collected versus applied voltage in a single wire gas chamber (from *Melissinos* [6.1])

4.1.1 Resistive plate chamber

- Two resistive plates with small gas gap ($\sim$ 2 mm) and large voltage on electrodes outside of the plates ($\sim$ 10 kV)
- Advantage: good time resolution $\sim 50 - 100$ ps
- Disadvantage: bad signal quality, dark rates

4.1.2 Ionization chamber

- Number of e^-/ion pairs produced is equal to number of ionizations by particle
- Current is typically quite low
- Can be used for experiments with large radiation fluxes

4.1.3 Proportional counter

- e^- from primary ionization drifts towards anode ($v \sim \mu$m/ns)
- $\vec{E}$-field is strong enough close to the anode that e^-s from ionization are accelerated and cause secondary ionizations
- These secondary ionization e^-s can also create tertiary ionizations, and so forth
- Occurs in the "avalanche region" close to the anode (since $|\vec{E}(r)| \propto 1/\ln(r/a)$), typically $r - a \lesssim 10$ μm
- Up to 10^6 amplification

4.1.4 Geiger-Müller counter

- ΔV is so high that an ionization sparks multiple avalanches along entire length of anode
  - e^-s from primary ionization are accelerated so strongly that when they hit an atom, they ionize it but also put the atom in an excited state
  - When the atom de-excites, it releases a γ, which initiates its own avalanche
  - Output current is independent of E
  - Need a quenching gas to absorb γs and shorten the signal pulse
- Obviously only useful for counting number of incident particles
- If $V_0 > 1$ kV, you get spontaneous breakdown of the gas, and it is no longer useful

4.2 Ionization and transport in gas

- Ionization mechanisms (assuming ψ is some charged particle):
  - $\psi + X \to \psi + X^*$ is a resonant process
    - In noble gases, $\sigma \sim 10^7$ b
  - $\psi + X \to \psi + X^+ + e^-$ is not resonant
    - $\sigma \sim 10^8$ b
    - Higher energy threshold than excitations (need to overcome valence binding energy)
- In general, σ is higher for low-energy transfers, so excitations dominate ionizations
- e^-/ion pairs produced by ψ can also create secondary e^-/ion pairs if energetic enough
  - Process repeats until E_{e^-} <ionization threshold

4.2.1 Mean number of e^-/ion pairs

- Note that the number of pairs is not equal to (energy lost)/(ionization energy), because some energy is lost through excitation of atoms
- In noble gases, 1 e^-/ion pair produced corresponds to ~ 30 eV energy lost
- For gaseous detectors, the Fano factor is typically ~ 0.2

4.2.2 Recombination and e^--attachment

- These processes eat up e^-/ion pairs before detection
- Recombination: if $\psi + X \to \psi + X^+ + e^-$, then we can have $X^+ + e^- \to X + \gamma$
  - Similarly, if two ions exist in the gas: $X^+ + Y^- \to XY + \gamma$
- Electron attachment: capture by electronegative atoms: $e^- + Y \to Y^- + \gamma$

4.2.3 Diffusion

- In principle, a charged particle in a detector will follow the $\vec{E}$-field lines
- But, it can be knocked about through elastic collisions with atoms
- Problem for detectors in which electrons must drift very far
- One way to minimize the effect is to add a parallel $\vec{B}$-field (so that if a particle is knocked off the field line, it remains in a tight helix). This is done in TPCs

4.3 Avalanche multiplication

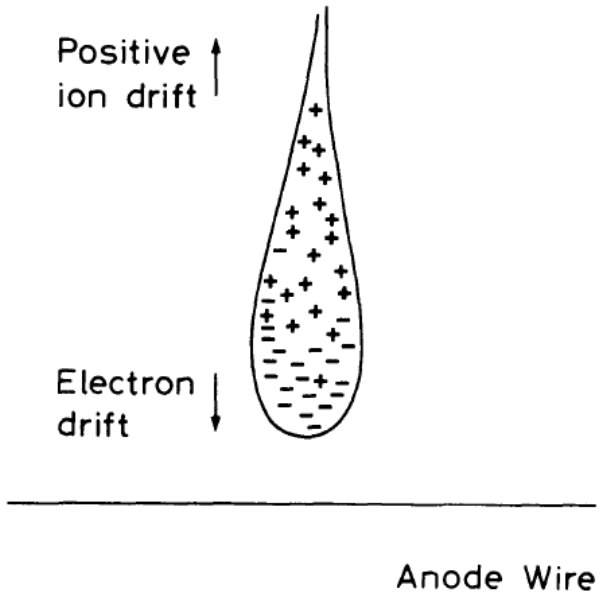

- The initial e^- has high energy and causes secondary, tertiary, etc ionizations
- e^-s move much faster than ions, giving the charge distribution a liquid drop shape
- Let λ be the mean free path of an e^- causing secondary ionization
  - $\alpha = \lambda^{-1}$ is the prob. of ionization/unit length

$$dn = n\alpha dx \tag{17}$$

where n is the number of free e^-. Then:

$$n = n_0 e^{\alpha x} \tag{18}$$

where n_0 is the number of primary ionizations

- $e^{\alpha x}$ is the proportionality factor in prop. counters

- Above calculation assumes a constant $\vec{E}$-field $\Rightarrow$ constant α
  - More generally:

$$e^{\alpha x} \to \exp\left[\int_{r_1}^{r_2} dx\ \alpha(x)\right] \tag{19}$$

4.4 Pulse formation and shape

- Consider a cylindrical proportional counter as an example
- Consider the counter as a coax capacitor with capacitance/unit length C
  - If a charge q moves by dr, then

$$dW = q\frac{d\phi}{dr}dr \tag{20}$$

    where W is the system energy and ϕ is the electric potential
  - For a capacitor of length L, $W = \frac{1}{2}LCV_0^2$, so

$$dW = LCV_0 dV \tag{21}$$

  - Equating:

$$dV = \frac{q}{LCV_0}\phi'(r)dr \tag{22}$$

  - That is, the motion of q by dr induces a measurable change in the potential
- $\Rightarrow$ observed signal is *not* charges collecting on the wire/wall, but an induced voltage change due to moving charges
- The total induced voltage change for a particle starting a distance r' from the wire is:

$$\int dV = \int_{a+r'}^{R} dr\ \frac{q}{LCV_0}\phi'(r) \tag{23}$$

  where $R = a$ ($R = b$) for e^- (ions).
  - Avalanches only occur when the $\vec{E}$-field is very high (close to the anode), so typically $r \sim \mathcal{O}(()1)$ μm ($a \sim \mu\text{m}, b \sim \text{mm}$)
  - i.e. $b - (a + r') \gg r'$ $\Rightarrow$ pulse is primarily caused by motion of positive charges
  - For many (but not all!) types of prop. counters, can ignore signal from e^-
- In the following figure, time starts with the beginning of the avalanche (drift time is ignored)

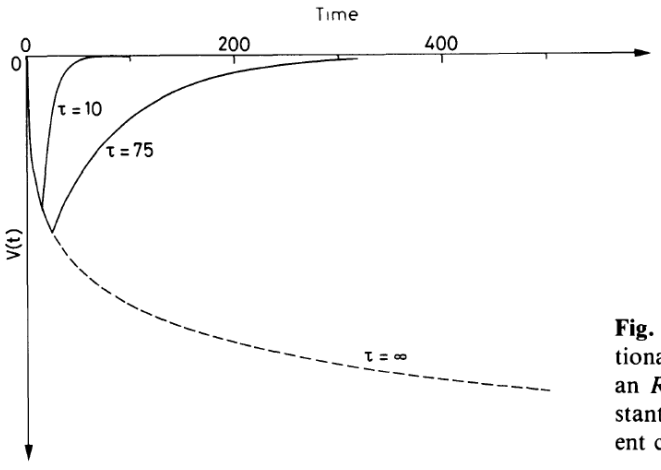

Fig. 6.6. Pulse signal from a cylindrical proportional counter. The pulse is usually cut short by an RC differentiating circuit with a time constant τ. The figure shows the effect of two different constants

4.5 Multiwire proportional chamber

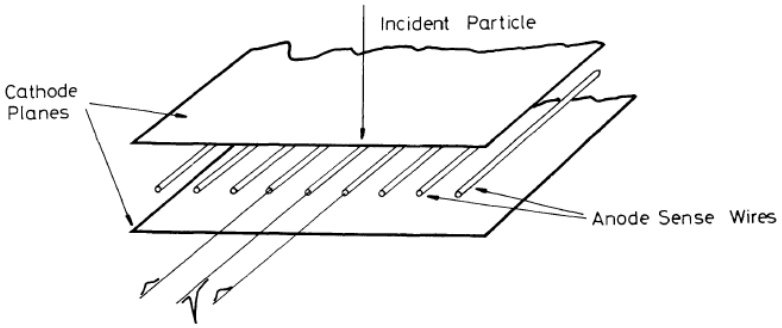

Fig. 6.7. Basic configuration of a multiwire proportional chamber. Each wire acts as an independent proportional counter. The signal on the firing wire is negative while the signals on the neighboring wires are small and positive

- Cathode planes are separated by ~ 10 mm and the wires are spaced ~ 2 mm apart
  - Spatial resolution is $\sim 1/2$ of wire spacing
- The efficiency of a particle creating a signal is typically $\sim 99\%$
- Free e^-/ions drift towards nearest anode wire/cathode wall
- Upon getting close to the anode, e^- can induce avalanche
- Ions from avalanche induce negative voltage difference on anode (same as proportional counter)
- Also induces a small *positive* signal on adjacent anodes
- Can align many MWPCs (with alternating layers at right angles) to determine trajectory
  - With sufficiently many such layers, can get 3D particle trajectory reconstruction

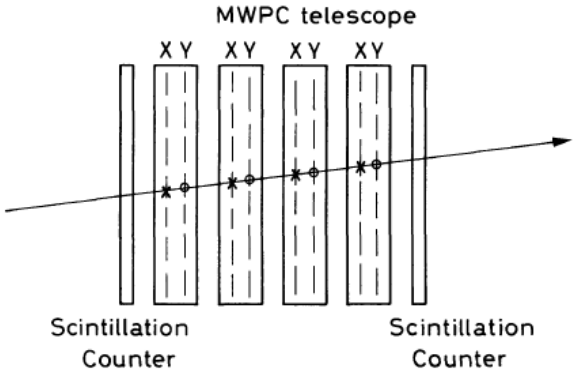

Fig. 6.9. A MWPC telescope for particle tracking. Each MWPC contains an X and Y wire plane. If the MWPC's are aligned, the measured coordinates allow a reconstruction of the particle trajectory. More than two planes of wires in a chamber may also be used

- Since each anode wire is a separate detector, MWPCs can detect multiple particles, as long as they do not overlap
- Magic gas: 75% Ar, 24.5% isobutane, .5% freon $\Rightarrow$ gains up to $\sim 10^7$
  - Argon is used because noble gases require smallest $\vec{E}$-field for avalanche
  - Above gains of $\sim 10^3$, argon atoms will become excited and then de-excite by releasing a γ $\Rightarrow$ can release photoelectric e^- in cathode
  - Add a quenching gas (isobutane) to absorb γs and dissipate energy thermally

  - Freon is added to kill any remaining dark current (i.e. electrons escaping from cathode due to high $\vec{E}$-field). Freon is very electronegative and therefore can capture low-energy e^-s

- If magic gas is used:
  - The signals are saturated and independent of energy $\Rightarrow$ can be used for position tracking
  - High gain $\Rightarrow$ signal from e^-s is measurable. This is much faster than the ion signal, giving better timing resolution $\sim$ 25-30 ns

- Multiple firings

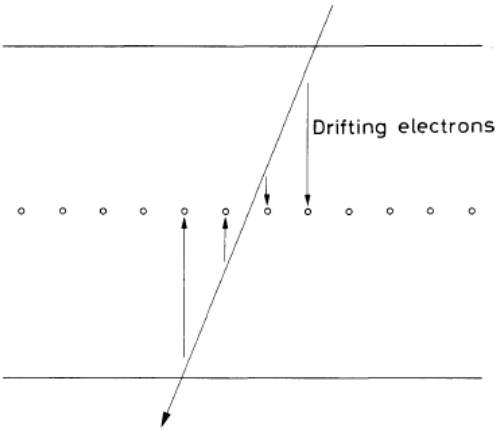

Fig. 6.13. Track clusters caused by particles arriving at an angle to the anode plane

  - The first and last ionizations in the diagram above will give delayed signals (wrt the second and third ionizations) because of the e^- drift time
  - Typically use this timing info to get the signal localized to one or two anode wires

4.6 Drift chamber

- Similar to proportional counter. Uses many "field wires" held at constant potential to ensure uniform $\vec{E}$-field
- Uniform $\vec{E}$-field $\Rightarrow$ constant drift velocity

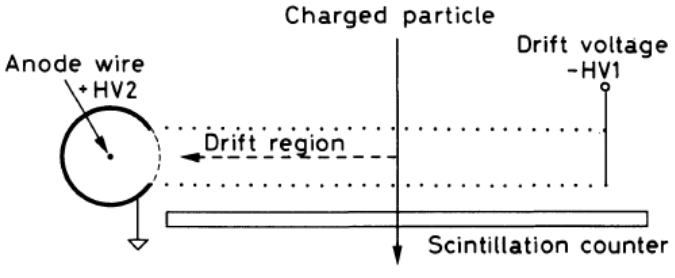

Fig. 6.15. Basic operating principle of the drift chamber (from *Sauli* [6.3])

- Operation:
  - Particle sets off scintillator. Timer starts
  - Particle ionizes an atom in chamber. e^- drifts to anode
  - e^- reaches (near) anode, inducing a signal through avalanche. Timer stops
  - Using Δt and constant drift velocity of e^-, position in z can be determined

- Spatial resolution is now determined by timing resolution of scintillator and anode signal
  - $\Rightarrow$ no longer need high wire density (like MWPCs)
- Max counting rate is $\sim 10^4/(\text{s}\cdot\text{mm})/\text{wire}$
  - Same as MWPCs, but fewer wires $\Rightarrow$ smaller flux can be handled

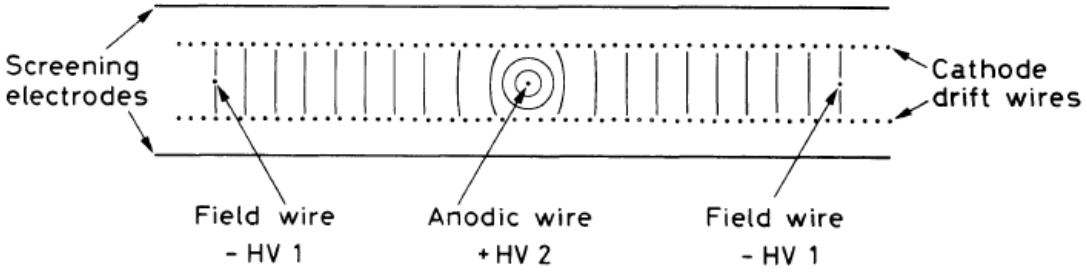

Fig. 6.16. Drift chamber design using interanode field wires (from *Breskin* et al. [6.22])

- Cylindrical drift chambers used at collider detectors
- Drift chamber is much more sensitive to gas composition, pressure, impurities, because all these things affect constant drift velocity assumption
- Correction needs to be made to account for presence of a $\vec{B}$-field
- Drift velocity of e^- is $\sim \mathcal{O}(10)$ μm/ns in Ar
- Higher drift velocity $\Rightarrow$ lower uncertainty from diffusion

4.7 Time projection chamber

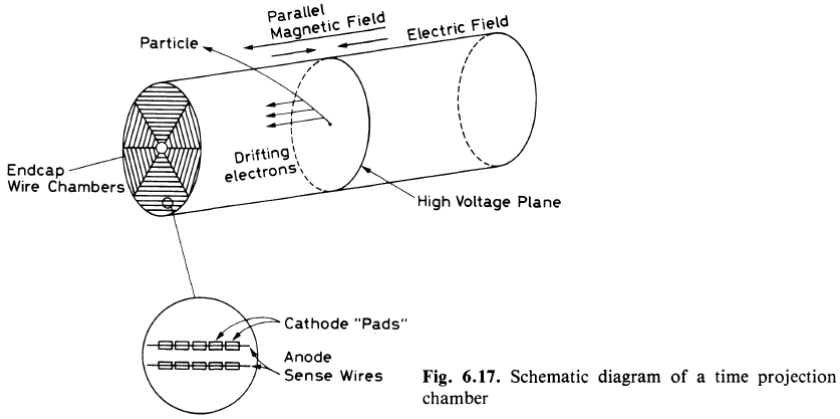

Fig. 6.17. Schematic diagram of a time projection chamber

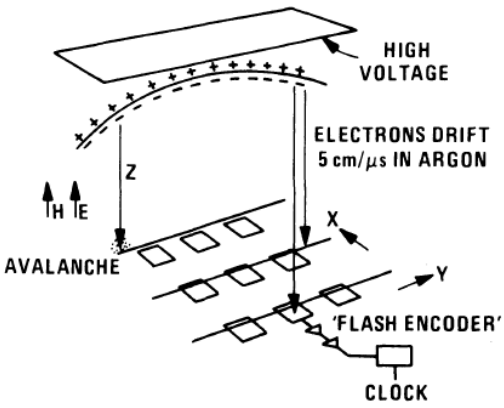

- Combines principles of a MWPC and drift tube, as well as giving info on particle momentum and dE/dx
- Constant $\vec{E}$-field $\Rightarrow$ electron drift velocity is constant
- $\vec{B}$-field has two purposes:
  - Curves tracks of charged particles
  - Ensures e^- diffusion (multiple scattering) is always helical towards endcap of TPC

- 3D reconstruction:
  - 1D from which anode wire gets a signal
  - 1D from which cathode pads get charge on them
  - 1D from drift time
- Typically add a grid held at ground potential right before endcap
  - Traps positive ions before they drift back to central cathode
- Charge/signal on cathode pads/anode wires is $\propto$ energy of drift e^- $\Rightarrow$ gives dE/dx of particle
- Curvature of charged particle gives the momentum
- Anode wire spacing is ~ 1 cm
- Scintillation (i.e. for LAr TPC)
  - Liquid argon better for number of reasons
    - Higher density than gas (good for low σ interactions like νN)
    - Scintillator
    - Very low electronegativity
  - If the gas (or liquid) is a scintillator, can add photodetectors to measure position along z axis
  - Can use this info to know where the ionization occured (instead of relying on drift time)

5 Scintillators

- Particle excites an atom/molecule, which then de-excites by releasing a γ
- Emitted light is picked up by a photodetector
- Features
  - Above energy threshold, scintillator response is $N_\gamma \propto E$. Since photomultipliers have $N_e \propto N_\gamma$, the total response is linear in E
  - Very short deadtime, very fast response
  - Can distinguish particle type based on pulse shape
- If $N(t)$ is the number of photons emitted at time t, it can be approximated as the sum of a fast and slow components:

$$N = A \exp\left[-\frac{t}{\tau_f}\right] + B \exp\left[-\frac{t}{\tau_s}\right] \tag{24}$$

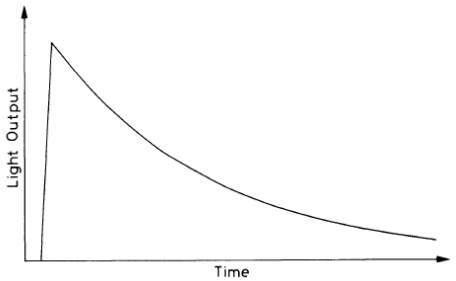

Fig. 7.2. Simple exponential decay of fluorescent radiation. The rise time is usually much faster than the decay time

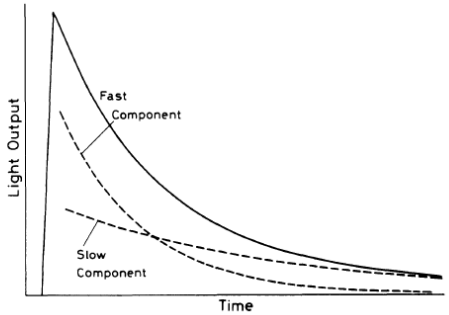

Fig. 7.3. Resolving scintillation light into *fast* (prompt) and *slow* (delayed) components. The *solid line* represents the total light decay curve

The values of A and B depend on the material and particle type (can be used for particle ID)

- Note that the above formula ignores the rise time (typically very short relative to the decay, so can be ignored).
- Desirable features:
  - High efficiency from energy lost to radiation
  - Transparency to radiation (so it can reach PMTs)
  - Emission range is in operating range of PMT
  - Short decay time τ
- Scintillators can be used as liquids or solids
- Liquid scintillators can be *loaded* with other things for specific purposes (e.g. Gd or B for high neutron capture σ)
- Energy loss ranges from 20 to 500 eV/photon

5.1 Organic scintillators

- Response time: $\leq$ few ns
- Molecules get excited
- Can have singlet (S_0) or triplet (T_0) spin ground state

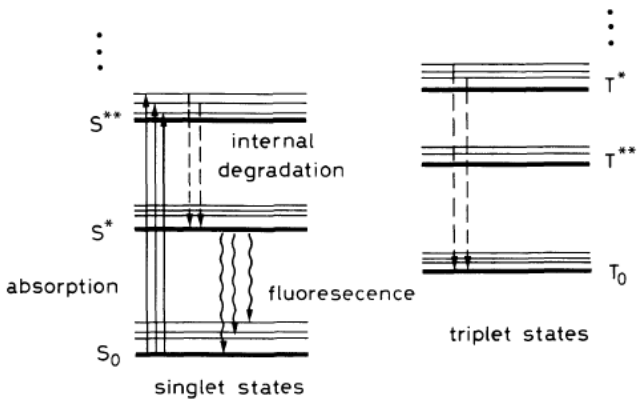

Fig. 7.4. Energy level diagram of an organic scintillator molecule. For clarity, the singlet states (denoted by S) are separated from the triplet states (denoted by T)

- S^* and S^{**} are electron excitations
- Excitation mechanism:
  1. Excitation goes from S_0 to S^{**} (or one of its vibrational excitations).
  2. Then, internal degradation to S^{**} (no γ released)
  3. Then, fluorescence to vibrational excitation of S_0 (or S_0 itself)
  4. Since bulk of atoms are in S_0, photons from de-excitation to vibrational excitation of S_0 will not be re-absorbed
- Similar story for triplet states, but $T_0 \to S_0$ is suppressed. Instead have $T_0 + T_0 \to S^* + S_0 +$ phonons
- Liquids have a response time of $\tau \sim 3 - 4$ ns

- Plastics
  - Organic apparently
  - Very fast response $\Rightarrow$ rise time cannot be ignored
  - $\tau \sim 2 - 3$ ns

5.2 Inorganic crystals

- Much slower $\tau \sim 500$ ns
- Main advantage is high stopping power because of high density and Z
- Higher light response (2-10×) than organics
  - $\Rightarrow$ better energy resolution
  - Useful for high energy γ or $e^{\pm}$
- Ex: NaI or $PbWO_4$
- Scintillation mechanism:
  - e^- can be excited from valence band to excitation or conduction bands
  - If excitation band, the e^--hole pair is in a bound state (exciton) that moves through the crystal
  - If the exciton hits an impurity, the e^- is absorbed by the impurity $\Rightarrow$ just a hole left behind
  - Then, an e^- passing by (from a higher energy state than the hole) will fill the hole, radiating a γ

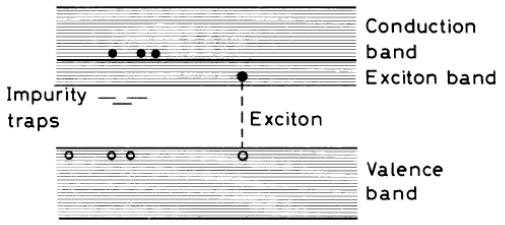

Fig. 7.7. Electronic band structure of inorganic crystals. Besides the formation of free electrons and holes, loosely coupled electron-hole pairs known as excitons are formed. Excitons can migrate through the crystal and be captured by impurity centers

5.3 Gas

- Very fast $\tau \sim 1$ ns
- Emits in UV range

5.4 Pulse shape discrimination for particle ID

- Fast and slow components of decay depend on dE/dx
- The components correspond to different de-excitations with different ΔE wrt ground state
  - Which excitations are populated is therefore dependent on dE/dx

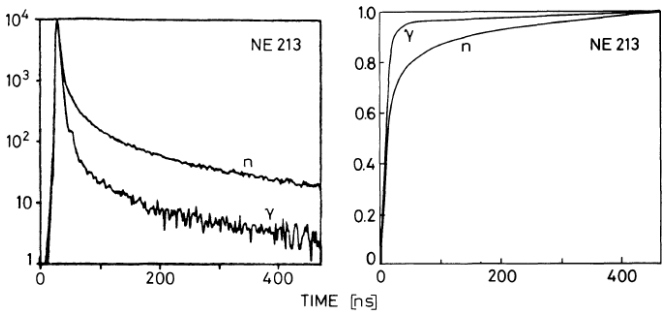

Fig. 7.12. Pulse shape differences of NE213 liquid scintillator light for neutrons and gamma rays. The time integral of the light pulses is also shown. A discrimination between these radiations may be obtained by measuring the time it takes for the integrated pulse to reach a certain fixed level (from *Lynch* [7.17]; picture © 1975 IEEE)

5.5 Quenching

- Energy lost through de-excitations that do not radiate a γ
  - e.g. through phonons or if the atom is ionized and the e^- is recaptured later
- Issue for heavy ions and αs, which heavily ionize
  - Inorganic scintillators used in this case, as they have a higher light output
- Quenching $\Rightarrow$ lower light output

5.6 Electron detection

- "Efficiency" close to 100%
- *However* if scintillator is high Z, may backscatter out of detector before depositing full energy
  - The 100% therefore refers to particles being counted, not energy measurement
- For low-to-medium $e^\pm$ energies, use low Z organic scintillators
- High Z inorganics good at high energy (facilitates EM shower production, depositing full energy)

5.7 Photon detection

- Want photoelectric and pair production (γ absorbed) to dominate Compton (γ scattered)
- $\sigma_{\text{photo}} \propto Z^5,\ \sigma_{\text{pair}} \propto Z^2,\ \sigma_{\text{Compton}} \propto Z$
- $\Rightarrow$ high Z is better for γs

5.8 Neutron detection

- High energy: look for recoil in $A + n \to B + p$
  - Organics good for this
  - Pulse shape to reject γ-backgrounds
- Thermal: use $A + n \to B + \gamma/\alpha$
  - Use things that have neutron capture σ: Li, B, Gd

6 Photomultipliers

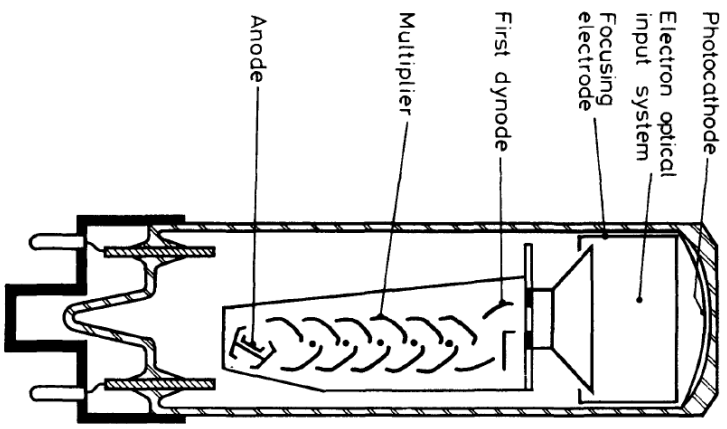

Fig. 8.1. Schematic diagram of a photomultiplier tube (from *Schonkeren* [9.1])

- Operation principle:
  1. γ hits cathode, ejects e^- through photoelectric effect
  2. e^- is accelerated to first dynode, where it knocks out multiple e^- s
  3. These are accelerated to the next dynode, each knocking out multiple e^- s, and so on
  4. Number of electrons reaching anode is roughly constant per photon
- Photon must typically be in narrow energy range (i.e. from scintillator)

6.1 Photocathode

- Quantum efficiency:

$$n(\lambda) = \frac{\#\text{ of photoelectrons released}}{\#\text{ of incident photons with wavelength } \lambda} \tag{25}$$

- Typically, semiconductors are used instead of metals (higher QE)
  - Suppose an e^- absorbs a γ and is traveling to the surface of the material
  - If material is metal, many interactions with free e^- s $\Rightarrow$ high dE/dx $\Rightarrow$ energy when it reaches surface may be too low to overcome potential barrier
  - Semiconductor e^- s are typically in valence bands or tightly bound $\Rightarrow$ low dE/dx

6.2 Multiplier dynodes

- Dynodes are made of insulator coating a conductor
- Typically 10-14 dynodes/tube
- Gains of 10^6-10^7

6.3 Gain and voltage supply

- Let V_d be the voltage between adjacent dynodes. The gain in N_e^- is $\delta = KV_d$, for some factor K
- The total gain, given N dynodes, is $G = (KV_d)^N$, assuming the same V_d for all dynode pairs

6.4 Pulse shape

- We assume the input photon distribution is from a scintillator with exponentially decaying response
- Then, the current is also exponentially decaying: $I = dQ/dt$, $Q = N_e \propto N_\gamma$

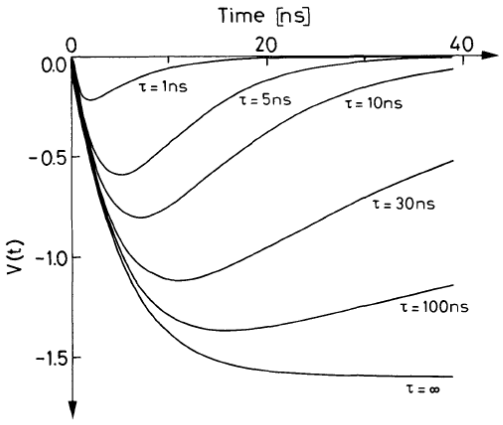

Fig. 8.13. Output signals for various time constants τ (after *Wright* [8.8])

6.5 Time resolution and response

6.5.1 Geometry of PMT

- Electrons from different parts of the cathode take different amounts of time to reach first dynode
- Spread in transit time is $\Delta t \sim 0.5$ ns. The transit time itself is $\sim$ 0.2-0.5 ns
- Above values are reached by using non-uniform $\vec{E}$-field between cathode and first dynode

6.5.2 Noise

- Dark current and after pulsing
  - DC is mostly from thermal noise
  - DC is exponential in $-\phi$ (work function); materials with $\phi < 0$ (good for PE effect) have high DC
  - Two sources of after pulses:
    - γ released from dynode when e^- hits. It can go back and release another e^- from the cathode
    - Ions created when e^- travelling through tube hits residual gas molecules. Ion travels back to cathode, release e^-
- Statistical noise
  - Due to statistical nature of PE effect
  - Fluctuations in the electron multiplier system
    - Statistical fluctuations in secondary emission
    - Difference in e^- transit times between dynodes

7 Semiconductor detectors

7.1 Basic principles

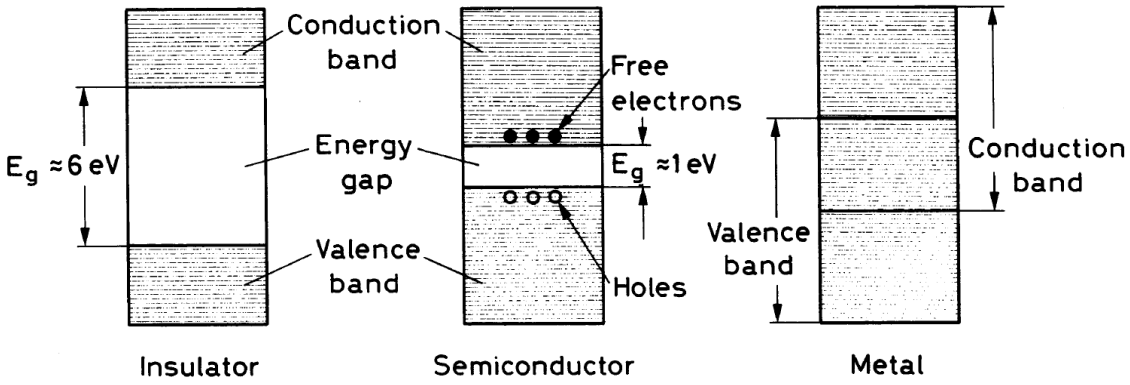

Fig. 10.1. Energy band structure of conductors, insulators and semiconductors

- Energy "bands" are actually many close, discrete energy levels $\Rightarrow$ treat them as continuous
  - Arise from degenerate latice energy levels breaking into many close discrete levels (due to Pauli principle)
- Below the valence band are tightly-bound e^- s
- Conduction band: free to roam in lattice
- Valence band: more tightly bound to individual atoms
- In an insulator, the bands are far apart. Im a semiconductor, the band gap is ~ 1 eV
- When a voltage is applied:
  - Insulator: valence e^- s are stuck $\Rightarrow$ no current
  - Metal: Thermally excited e^- s are in the conduction band $\Rightarrow$ current flows
  - Semiconductor: only a few e^- s in the conduction band, so a small current is observed. As $T \to 0$, the current decreases
- Charge carriers in semiconductors
  - Thermal excitation: e^- jumps to conduction band, leaving hole behind
    - Conduction band e^- can move freely $\Rightarrow$ one current
    - Valence band can also move freely $\Rightarrow$ another source of current
    - Hole current is due to e^- s moving around to fill holes
    - In contrast, metals only have one type of current (free e^-)
  - Number of e^-/hole pairs is $\propto T^{3/2} \exp\left[-E_g/2kT\right]$, where E_g is the energy gap size at 0 K
- Recombination
  - Process of e^- +hole$\to$phonon
  - Expect e^-/hole lifetime ~ 1 s
    - Long because in order for recombination to occur, e^- and hole must be in specific energy/momentum configuration
  - Experimentally, find $\tau \sim 1$ μs-100 μs $\Rightarrow$ some other mechanism of destroying pairs

– Impurities can add energy levels in the energy gap

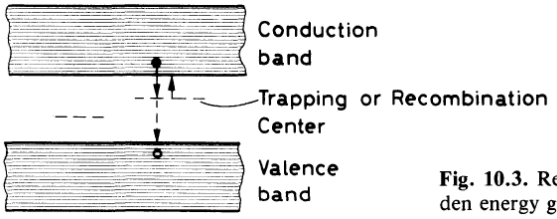

Fig. 10.3. Recombination and trapping sites in the forbidden energy gap

* These intermediate states can capture an e^- and later capture a hole (or vice versa), causing recombination
* Very efficient process
* Bad for detection, as it reduces charge carrier lifetime (i.e. recomb. occurs before the charges can be collected)
* Detectors need $< 10^{10}$ impurities/cm^3

– Trapping

* Similar to recombination impurities, except the extra energy states are charge-specific (i.e. only e^- or holes, but not both)
* Charge is then released after some characteristic time
  · If the capture time is longer than charge collection time, signal can be lost to trapping centers

– Recomb. and trapping effects can arise from structural defects in lattice as well

7.2 Doped semiconductors

- A semiconductor can be doped when a lattice atom is replaced with an atom with:
  – An extra e^- $\Rightarrow$ donor (n-type) impurity
  – A missing e^- $\Rightarrow$ acceptor (p-type) impurity
- For example, if the semiconductor is Si or Ge (quadravalent atoms), a donor would have 5 valence e^- (e.g. P), and an acceptor would have 3 valence e^- (e.g. Al)

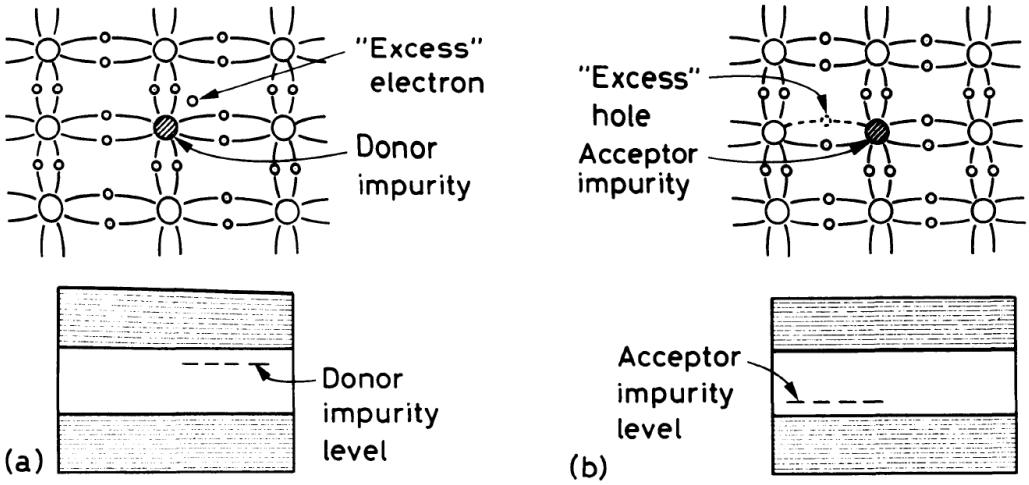

Fig. 10.4. **(a)** Addition of donor impurities to form n-type semiconductor materials. The impurities add *excess* electrons to the crystal and create donor impurity levels in the energy gap. **(b)** Addition of acceptor impurities to create p-type material. Acceptor impurities create an *excess* of holes and impurity levels close to the valence band

- n-type (i.e. extra e^-)
  - Valence band is filled up, so extra e^- creates an energy level in the gap
  - The ΔE between the impurity state and the conduction band is $\mathcal{O}(0.01)$ eV
  - This extra e^- is very easily thermally excited into conduction band $\Rightarrow$ better conductivity
  - Extra e^- will also drop down to fill holes $\Rightarrow$ hole current is somewhat suppressed
- p-type (i.,e. missing e^-)
  - Essentially everything said about n-type, but $e^- \longleftrightarrow$ hole.
  - Impurity level is very close to valence band (i.e. location of hole current)
- Let p, n be the concentrations of positive, negative (i.e. holes, free e^-) charges respectively; N_D, N_A be the concentrations of donor, acceptor impurities. Then, electric neutrality implies:

$$N_D + p = N_A + n \tag{26}$$

- Note that donors are positively charged: extra e^- is not in valence band (so it is counted as part of n). Inverse is true for acceptors

7.3 The np junction and depletion zone

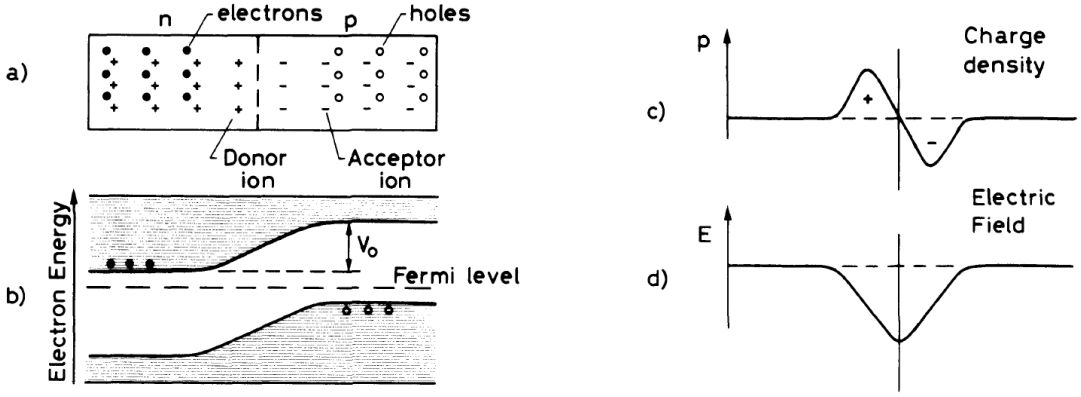

Fig. 10.5. (a) Schematic diagram of an np junction, **(b)** diagram of *electron* energy levels showing creation of a contact potential V_0, **(c)** charge density, **(d)** electric field intensity

- Basic concept: p-type semiconductor next to n-type material (actual fabrication is more complicated)
- n- and p-sides start neutral, but then:
  - e^- flow from n to p, filling holes
  - Holes from p to n, accepting e^-
  - $\Rightarrow$ result: p-side has static negative charge; n-side has static positive charge
  - Static charge distributions are localized near boundary
- Generates an $\vec{E}$-field from n to p. **IMPORTANT**: sign of $\vec{E}$-field in above diagram (from Leo) is incorrect
- The $\vec{E}$-field is equiv to a potential difference across junction ($V_0 \sim 1$ V)
- Non-zero $\vec{E}$-field pushes the energy levels up (down) on the p (n) side
  - Remember: e^- move against $\vec{E}$

  - More negative static charges on p-side $\Rightarrow$ e^- energy levels go up
  - More positive static charges on n-side $\Rightarrow$ e^- energy levels go down
- Capacitance: the electrostatic configuration resembles a plate capacitor with $C \sim \text{pF/mm}^2$
- Depletion zone
  - Area in which there are no free charges
  - Depth of n- and p-sides (calculation is below):

$$x_n = \sqrt{\frac{2\epsilon V_0}{eN_D(1+N_D/N_A)}}, \quad x_p = \sqrt{\frac{2\epsilon V_0}{eN_A(1+N_A/N_D)}} \tag{27}$$

  - $\Rightarrow$ if one side is more heavily doped than the other, the depletion zone extends further into the lightly-doped side
  - Depth calculation:

Assume the charge density is constant:

$$\rho(x) = \begin{cases} -eN_D & 0 < x < x_n \\ -eN_A & -x_p < x < 0 \end{cases} \tag{28}$$

Charge conservation implies $x_n N_D = x_p N_A$. Using Poisson's equation:

$$\phi''(x) = -\rho(x)/\epsilon \tag{29}$$

Integrating twice and choosing constants:

$$\phi(x) = \begin{cases} -\frac{eN_D}{\epsilon}\left(\frac{x^2}{2} - x_n x\right) & x \in n \\ \frac{eN_A}{\epsilon}\left(\frac{x^2}{2} + x_p x\right) & x \in p \end{cases} \tag{30}$$

Imposing $\phi(-x_p) = 0$ and $\phi(x_n) = V_0$ allows us to solve for the depths.

7.4 Semiconductors as detectors

- Principle: constant $\vec{E}$-field in depletion zone carries away charges from ionizaton
  - Holes go to p-side
  - e^- go to n-side
- Average energy to create e^-/hole pair is 3 eV
  - Can contrast with gases $\sim$ 30 eV
  - Scintillators are $\sim$ 300 eV
- For light particles ($m \lesssim m_p$), energy per ionization w is independent of particle type
  - Therefore, given a collection efficiency n, particle of energy E, and assuming the particle is stopped in the semiconductor:

$$Q = \frac{nE}{w} \tag{31}$$

  - Not quite true for heavier ions $\alpha, \ldots$
- What is measured is a voltage difference induced by charge collected Q $\Rightarrow$ $V = Q/C$

7.4.1 Reverse bias

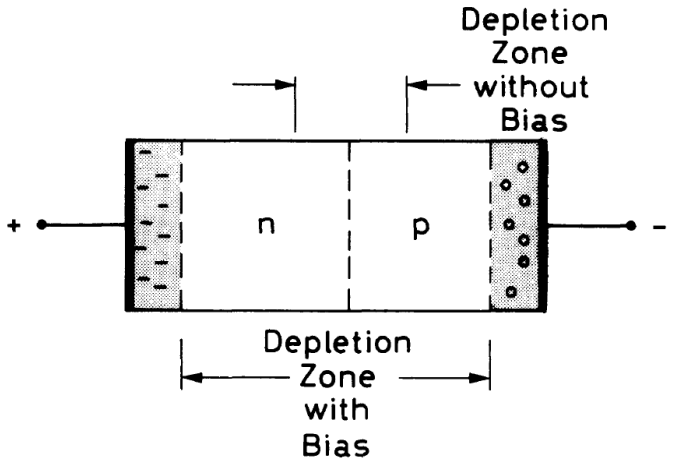

Fig. 10.7. Reversed-bias junction

- Normal depletion zone is rather small and $\vec{E}$-field is relatively weak
- Fix both issues by adding an additional bias voltage $V_B \gg V_0$
- Note: V_B is maintained and $V_B \gg V_0$, so changing V_0 due to individual ionizations is negligible
- Can get depletion zones of ~ 1 mm

7.4.2 Detector characteristics

- Fano factor is $\sim 0.12 \Rightarrow$ energy resolution for a 5 MeV particle is $\sim 0.07\%$
- Response is very fast ~ 10 ns, and timing resolution can get down to ~ 10 ps
  - Drift time is ~ 10 ps/μm in silicon
- Dimensions are typically ~ 100 μm $\Rightarrow$ spatial resolution is dimension divided by $\sqrt{12}$

7.5 Silicon strip detectors

- Same basic principle as the detectors described above, just in a different geometry

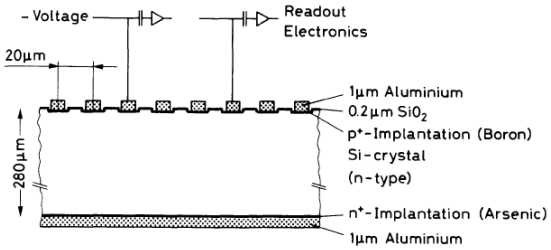

- p-type strips embedded in n-type bulk
- Thickness is typically ~ 300 μm. Can get much larger depletion zone
- Spatial resolution is better than spacing of strips: can use the amount of charge deposited on each strip to interpolate where the ionization happened
  - $\Rightarrow$ $\sigma \sim 5$ μm if the spacing is 20 μm
  - Typically factor of 3-7$\times$ improvement

7.6 Silicon photomultipliers

- Like with PMTs, the photon hits a semiconductor (such as silicon dioxide) and ejects a photoelectron
- If the bias voltage is large enough, the pair can cause secondary ionizations $\Rightarrow$ avalanche
- In Geiger mode, can get gains of ~ 100
- CMS ECAL avalanche photodiodes have a total efficiency (quantum times collection) of 70%
- A SiPM is a large array of APDs in Geiger mode
  - Downside is large dark rate

8 Compact Muon Solenoid

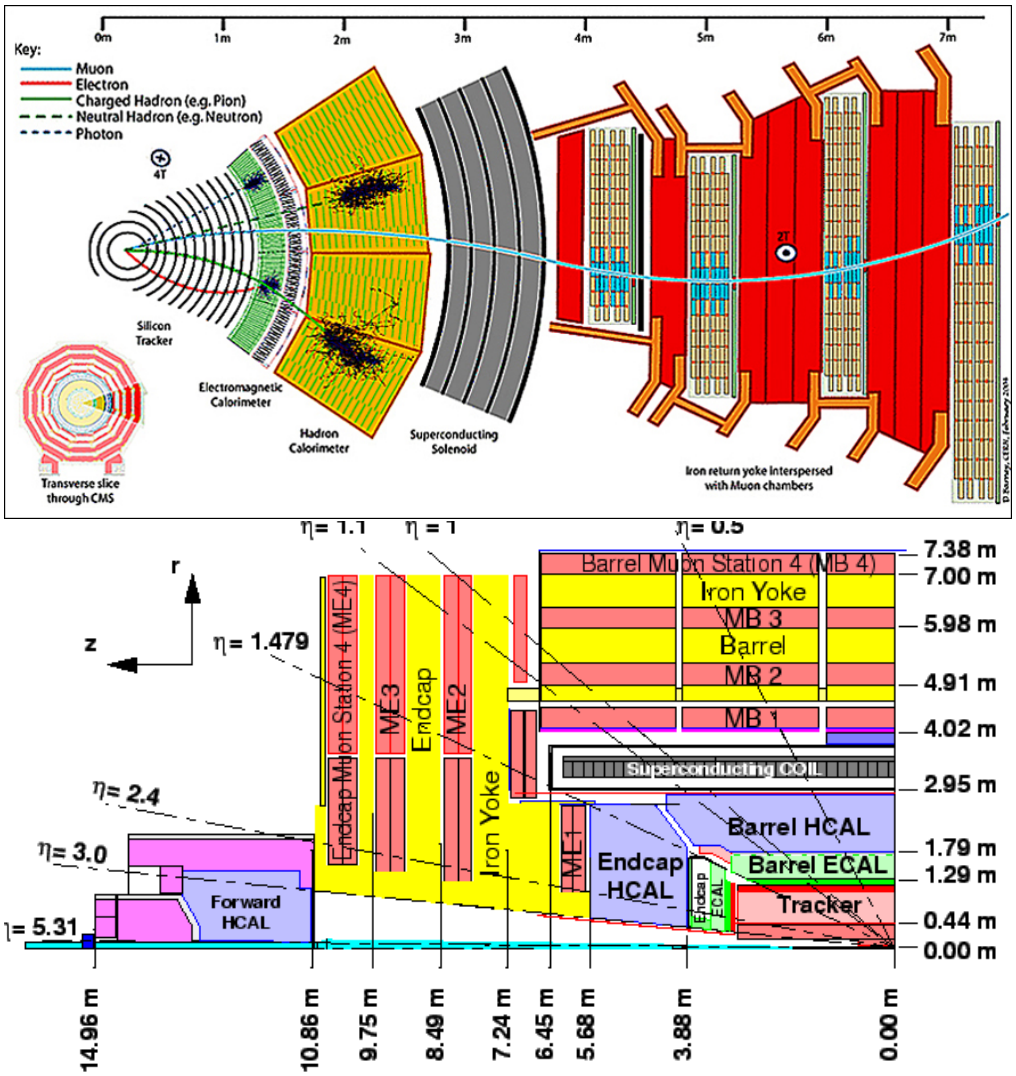

8.1 Silicon tracker

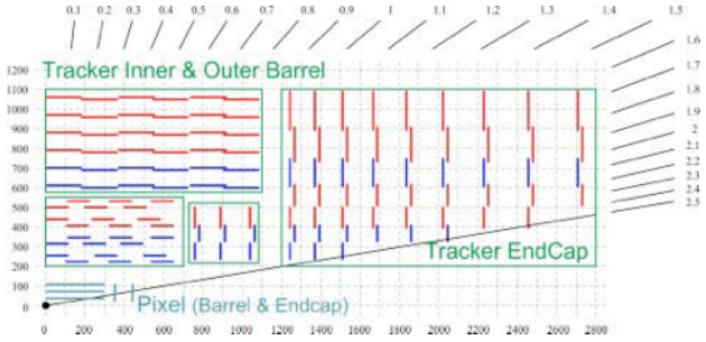

- Reasons to use a silicon tracker:
  - Fine granularity and fast response time
  - Radiation resistant
  - $\sim 1\%$ resolution at $p_T = 100$ GeV
  - Can measure impact parameter of tracks (i.e. vertexing) very well: $\sigma_{\text{IP}} \sim 20$ μm
- Lorentz drift of charges
  - Drift of charges in detectors is affected by $\vec{B}$-field
  - Can lead to charge sharing: multiple pixels set off by a single hit
  - *If reconstructed properly*, can actually improve spatial resolution (i.e. the amount of charge sharing can tell you how close to the edge of the pixel the interaction occurred)
  - The angle of deflection due to the Lorentz effect has been found to increase as a function of radiation damage
- Hit reconstruction efficiency is very high: 99.5% (99%) in pixels (strips)
- Total radiation length ranges from $0.5\times$ to $2 \times X_0$
  - Lowest at low η

8.1.1 Inner pixel detector

- Detector specification:
  - 66 million silicon pixels
  - 100 μm $\times$ 150 μm $\times$ 285 μm pixels
  - Three barrel layers at radii of 4.3, 7.2, and 11 cm
  - Two endcap disk layers at z of 35 and 46 cm
  - Position of layers guarantees at least 3 hits (not accounting for detector efficiency) for $|\eta| < 2.5$
- Flux of particles is 10^6 cm^{-2}s^{-1}
- Hit reconstruction
  - Readout threshold is 3.2k electron-equivalent charges
  - Offline, define a pixel cluster as adjacent (either sharing a side or corner) pixels containing at least 4k electrons

  - MIP typically deposits 20k electrons
  - Position of particle within cluster determined by using charge distribution
  - Resolution of hit is $\sigma_{r\phi} \sim 10$ μm and $\sigma_z \sim 30$ μm
- Radiation damage can be assessed and corrected for by looking at the mean response as a function of time
- Occupancy is typically 10^{-4}-10^{-3} per channel
  - Particle density is higher than in the outer detector, but occupancy is lower because of granularity

8.1.2 Outer strip detector

- Detector specification:
  - 9 million p-type strips embedded into a n-type bulk (thickness $\sim$ 320-500 μm)
  - Like the inner detector, consists of multiple barrel and endcap disk layers
  - About half the layers are 1D (i.e. provide only $r\phi$ measurement) and the other half are 2D (giving 3D position measurement)
  - Ranges from 25 cm to 110 cm in r and up to 120 cm (280 cm) in z in the barrel (endcap)
  - Strip lengths are 10-20 cm. Strip pitch (spacing) is 80-205 μm
    * Things are finer in the innermost layers
- Occupancy ranges from 10^{-3} to 10^{-2}
- Use charge-weighted average to determine position of hit
  - Spatial resolution is therefore $\sim$ 20-50 μm

8.1.3 Track reconstruction

- Iteratively do pattern recognition and track fitting using a combinatorial Kalman filter
  - First look for high p_T tracks (easiest to reconstruct), then remove these hits and repeat until all hits are associated with a track or classified as noise
  - 6 such iterations are done at CMS
- Each iteration does 4 things:
  - First, generate track seeds using collections of 2-3 hits in the pixel detector and estimate trajectory parameters from this seed
  - Extrapolate the track from the seed using a Kalman filter and search for hits consistent with the extrapolation
  - Run a track fitting procedure to get best estimate of trajectory parameters and covariance matrix
  - Discard tracks that fail quality requirements (i.e. too many missing hits, bad χ^2,...)
- The trajectory parameters take into account several effects:
  - Curvature due to $\vec{B}$-field
  - Change in path from multiple scattering (can be difficult to do if angle is large for a high p_T track)
  - Change in curvature due to dE/dx
- Electron tracking

  - Electrons lose a lot of energy in tracker due to brem: up to 70%. Energy loss is very non-Gaussian
  - Use additional ECAL info to build electron tracks
    * For example, look for ECAL clusters from the brem photons

- Tracking efficiency is $\gtrsim 90\%$ ($\gtrsim 99\%$) for electrons and pions (muons) if $p_T > 10$ GeV is required
- Resolution on p_T ranges from 1% to 10%, as a function of p_T, η:

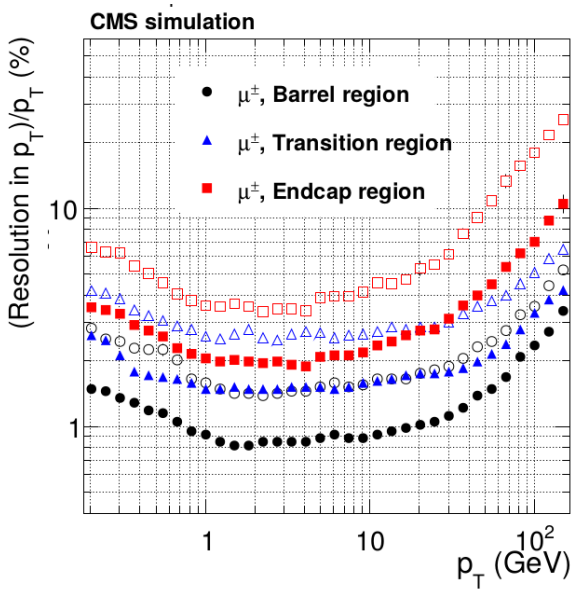

8.1.4 Vertex reconstruction

- Primary vertex resolution is $\sim \mathcal{O}(10)$ μm and depends on the number of tracks:

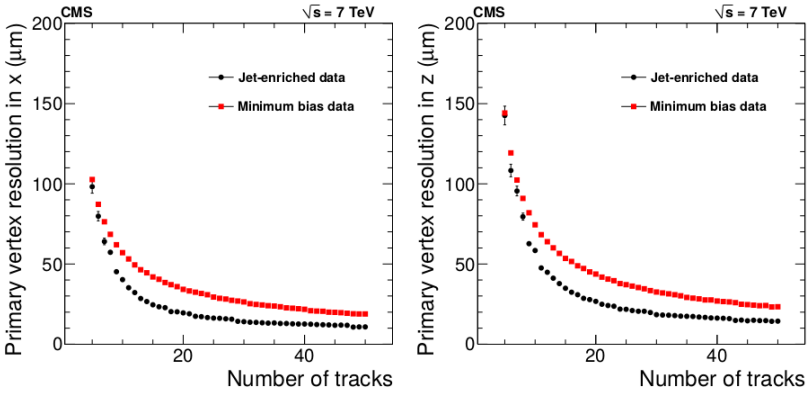

  - Efficiency is > 0.995 if at least 3 tracks are present

- Similarly, can use tracks with high impact parameter to reconstruct secondary vertices (decays of B mesons, K^0, $\gamma \to e^- e^+$). Resolution is similar to PVs

8.2 Electromagnetic calorimeter

- Two components: barrel ($|\eta| < 1.479$) and endcap ($1.653 < |\eta| < 3.0$)
  - Preshower coverage for endcap ends at $|\eta| < 2.6$

- Made out of lead-tungstate crystals ($PbWO_4$)
  - $X_0 = 0.89$ cm and $R_M = 2.2$ cm. These are quite small
  - Response times are $\tau_f = 10$ ns and $\tau_s = 25$ ns
    - This is an order of magnitude better than other inorganic scintillators
  - Emits light at 420 nm
- ECAL is a homogeneous calorimeter: single crystals that act as the absorber and detector
  - Advantage: very good energy resolution
  - Disadvantage: expensive and no longitudinal shower information

8.2.1 Barrel configuration

- 61k crystals of dimension $R_M \times R_M \times 26X_0$
- Each crystal has dedicated APD, operated in linear mode (gain of 50)
- QE of APDs is 80%

8.2.2 Endcap configuration

- 14k crystals of dimension $1.3R_M \times 1.3R_M \times 25X_0$
- Each crystal has a dedicated vacuum phototriode, operated in linear mode (gain of 10)
  - QE is 20%
  - Use VPT instead of Si APD because of radiation hardness requirements
  - Response is very fast: 1 ns
  - Honestly, there are some things about VPT operation that I do not understand. Yutaro was also unsure. Probably unimportant...
- Preshower detector
  - At high η, a $\pi^0 \to \gamma\gamma$ decay might be boosted enough that the photons overlap in the ECAL
  - The preshower is two layers of Pb+Si detectors with a spatial resolution of 2 mm $\Rightarrow$ can distinguish γ from $\gamma\gamma$
  - This detector is right before endcap ECAL

8.2.3 Electron and photon reconstruction

- Most particles deposit all energy within 3×3 box of crystals
- Particles are seeded using ECAL superclusters
  - Start with some pre-defined seed of crystals (such as one high-energy crystal)
  - Then add adjacent crystals to the supercluster if they also have high energy
- Center of the cluster is defined by log-weighting the energy
- For photons, the energy is defined by looking at a 5×5 cluster
- Electron-initiated showers are wider due to brem, so the energy is defined as the total energy of the supercluster

- Distinguishing between a e and γ (or charged hadrons) can be done using the η-ϕ shape of the shower
  - Also only an electron should have 1 track, conversion have 2 tracks, charged hadron have HCAL deposit, etc...

8.2.4 Energy resolution

- The energy resolution in the barrel is:

$$\frac{\sigma_E}{E} = \frac{2.8\%}{\sqrt{E\ [\text{GeV}]}} \oplus \frac{0.128}{E\ [\text{GeV}]} \oplus 0.3\% \tag{32}$$

  It is slightly worse in the endcap
- ECAL is instrumented with lasers of known energy to constantly monitor resolution
- Photon energy resolution is ~ 1 GeV at $p_T = 100$ GeV
- Resolution of $m_{\gamma\gamma}$ in Higgs discovery was $\sim$ GeV. This is determined by:
  - Energy resolution of each photon
  - Position resolution of superclusters (so opening angle can be measured)

8.3 Hadron calorimeter

- 4 components:
  - $|\eta| < 1.39$: Barrel
  - $1.30 < |\eta| < 3.00$: Endcap
  - $2.85 < |\eta| < 5.19$: Forward
  - $|\eta| < 1.30$: Outer
- Note that, unlike the ECAL, there is no gap until the end of the detector
  - Necessary for good $\not{E}_T$ resolution, since most particles in an event are hadrons
- HO is outside the solenoid; other components are inside
  - Inside solenoid reduces material budget before detector $\Rightarrow$ better energy resolution
  - However, limited size of solenoid $\Rightarrow$ thickness of HB is only $\sim 6\lambda_I$ (where λ_I is the nuclear interaction mean free path)
  - HO is used to extend this
- Light collection done using hybrid photodiodes

8.3.1 HCAL Barrel

- Consists of 1 steel layer, 14 brass layers, and another steel layer
  - λ_I for brass is 16.4 cm
  - Total depth is equivalent to $5.9\lambda_I$
  - Each brass layer is ~ 50 mm thick
  - Absorber layers are interleaved with plastic scintillator

- Segmented into η-ϕ towers of 0.087×0.087 radians
- Small thickness $\Rightarrow$ stochastic term dominates energy resolution:

$$\left(\frac{d\sigma_E}{dE}\right)_{\pi^0} \approx \frac{0.9}{\sqrt{E\ [\text{GeV}]}} \tag{33}$$

8.3.2 HCAL Endcap

- Also brass and steel
  - Total depth is equivalent to $10\lambda_I$
- Also segmented into η-ϕ towers of 0.087×0.087 radians
- Pion energy resolution:

$$\left(\frac{d\sigma_E}{dE}\right)_{\pi^0} \approx \frac{1}{\sqrt{E\ [\text{GeV}]}} \tag{34}$$

8.3.3 HCAL Forward

- Iron absorbers interleaved with quartz
  - Total depth is equivalent to $10\lambda_I$
  - Collect Cerenkov light from quartz
- Segmented into 36×13 towers in the $\phi \times \eta$ plane

8.3.4 HCAL Outer

- Uses the solenoid and first yoke layer (mostly aluminum and iron, respectively) as absorbers
  - Total depth is equivalent to $10\lambda_I$
  - Layer of scintillator after each absorber
- Pion energy resolution:

$$\left(\frac{d\sigma_E}{dE}\right)_{\pi^0} \approx \frac{1.2}{\sqrt{E\ [\text{GeV}]}} \tag{35}$$

8.3.5 Jet energy resolution

- The reconstructed objects of the HCAL are jets
  - Reconstruction uses tracking and ECAL information as well
- Uncertainty in p_T is at worst 7% and is better than 1% for central, high p_T jets:

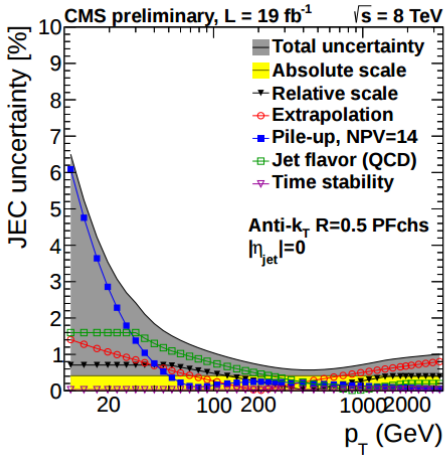

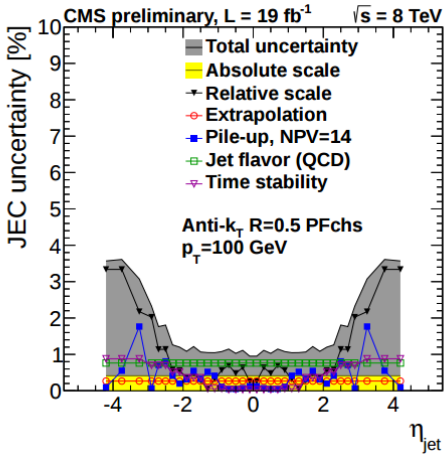

- Calibrating jet energy scale is very important as it controls the uncertainty on the $\not{E}_T$

8.4 Magnet and return yokes

- Magnet is a solenoid generating a 3.8 T field inside
- Coil is a superconducting alloy. Maintained at 4 K using LiHe
- It uses a lot of aluminum to stabilize the superconducting coil
- Superconducting coil is NbTi
- Radius of solenoid is 3 m
- Outside the solenoid:
  - $\vec{B}$-field is in the opposite direction and has strength ~ 2 T
  - $\vec{B}$-field is guided using 4 iron return yokes

8.5 Muon detectors

- Magnet return yokes are used to shield muon detectors from punch-through hadrons
- Three components:
  - Drift tubes: $|\eta| < 1.2$
  - Cathode strip chambers: $0.9 < |\eta| < 2.4$
  - Resistive plate chambers: $|\eta| < 2.1$

8.5.1 Drift tubes

- 240 drift tube chambers over $|\eta| < 1.2$
- Organized radially in 4 stations, with the return yoke interspersed
  - Each station has multiple drift tubes in it
  - Note these station also have RPC detectors (discussed below)
- Each station has three superlayers of DTs:

  - 2 superlayers consisting of 4 layers each that the ϕ position
  - 1 superlayer consisting of 4 layers that gives the z position
- Drift gas is argon (85%) and CO_2 (15%)
- Maximum drift time is 400 ns
  - Resolution on drift time is 1 ns
- Each chamber (i.e. layer) has a spatial resolution 100 μm in the value of ϕ-z plane

8.5.2 Resistive plate chambers

- 612 RPCs
  - 6 stations in the barrel
  - 4 stations in the endcaps
- Operated in avalanche mode
- Gap width is 2 mm
- Gas is mostly $C_2H_2F_4$
- Timing resolution is very good: 3 ns

8.5.3 Cathode strip chambers

- Used in the barrel because it can handle higher fluxes
- Total of 6 endcap stations
- Essentially a proportional counter, except each chamber is instrumented with multiple anode wires and cathode strips
  - Anodes and cathodes are perpendicular to each other
- Muon creates a primary ionization which induces an avalanche. Ions move to cathode and electrons to anode, giving 2D spatial reconstruction
- Spatial resolution os 100 μm and timing resolution is 3 ns

8.5.4 Muon reconstruction

- Can identify a standalone muon (using just the muon chambers) or a global muon (adding tracker info)
  - Note tracker gives complementary information, since $\vec{B}$-field changes direction
  - Below 200 GeV, tracker dominates accuracy, since multiple scattering in solenoid and yoke messes up measurement in muon chambers
- Global muon reconstruction efficiency is $\gtrsim 97\%$
- Global muon p_T uncertainty is less than 1% for $p_T < 100$ GeV:

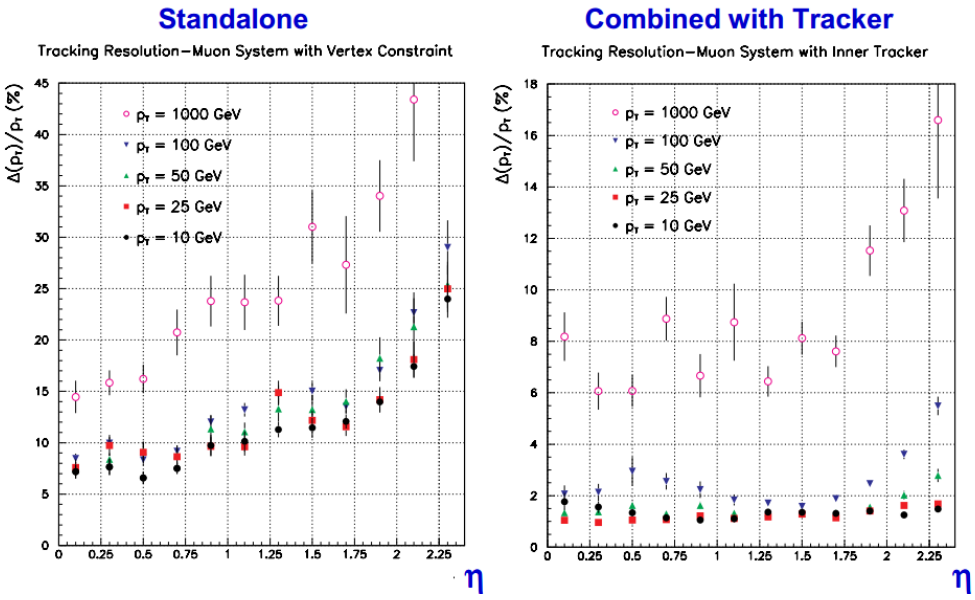

8.6 Triggering and DAQ

- LHC Run II luminosity is 10^{34} cm^{-2}s^{-1} and inelastic pp scattering cross section is 70 mb, so the event rate is $\sim 10^9$/s
- Each bunch crossing has an average of 22 overlaid events. Bunch crossing rate is 40 MHz
- If each event is $\sim$ 1 MB, then the data output is over 1 TB each second
  - Way too high to write out using existing implementations (although I believe DarkLight is aiming for this order of magnitude)
- Two stages: L1 and HLT
- Level 1 trigger system
  - Uses muon and calorimeter information to select interesting events
  - Can construct primitives like muons, electrons, photons; can also measure global variables like E_T, H_T, $\not{E}_T$
    - Use faster, but less accurate, reconstruction methods than what is used offline
  - Three components:
    - Global calorimeter trigger
    - Global muon trigger
    - Global trigger (takes info from GCT and GMT)
  - Reduces event rate from 40 MHz to 50 kHz
  - Functions by keeping events in buffer ("front-end pipeline") for a few microseconds. Event processing time is about 1 microsecond
  - Calculation is done online using FPGAs
  - Proposals for future is to add tracking information to L1 trigger: use fast pattern recognition to reconstruct track primitives for triggering
- High Level Trigger system
  - Each HLT path is "seeded" by a L1 trigger

    - For example, a HLT path that looks for b-tagged jets would be seeded by an L1 trigger with requirements on H_T
  - Reduces event rate down to $\mathcal{O}(100)$ Hz
    - At most 90% is used for actual physics; rest is dedicated for detector calibration
  - Decisions are made using information from all detector components
  - However, reconstruction is only partial, to reduce CPU time
    - Objects are reconstructed following objects that are identified by corresponding L1 trigger
  - Three levels within HLT:
    - Level 2.0: still no tracking information. Does stuff like construct ECAL superclusters. $\mathcal{O}(100)$ ms
    - Level 2.5: primitive tracking and vertexing using only pixels. $\mathcal{O}(10)$ ms
    - Level 3.0: using full tracker. $\mathcal{O}(100)$ ms
  - Average processing time ranges from 50 ms (jets+$\not{E}_T$) to 700 ms (muons)

Appendices

A Bibliography

The CMS Collaboration, *Description and performance of track and primary-vertex reconstruction with the CMS tracker*. arXiv:1405.6569

The CMS Collaboration, *The Magnet Project Technical Design Report*. CERN/LHCC 97-10

The CMS Collaboration, *Performance of CMS muon reconstruction in pp collision events at* $\sqrt{s} = 7$ *TeV*. arXiv:1206.4071

The CMS Collaboration, *Energy calibration and resolution of the CMS electromagnetic calorimeter in pp collisions at* $\sqrt{s} = 7$ *TeV*. arXiv:1206.2016

The CMS Collaboration, *Performance of jets at CMS*. 2015 J. Phys.: Conf. Ser. 587 012004

The CMS Collaboration, *Operation and performance of the CMS tracker*. arXiv:1402.0675

The CMS Collaboration, *The CMS High Level Trigger*.

The CMS Collaboration, *The CMS ECAL performance with examples*. 2014 JINST 9 C02008

Leo, W. R., *Techniques for Nuclear and Particle Physics Experiments*. Second Revised Edition

PDG Particle Review, *Passage of Particles Through Matter*. 2014 edition

PDG Particle Review, *Particle Detectors at Accelerators*. 2015 edition